NAVAL POSTGRADUATE SCHOOL
Monterey, California

THESIS

A FINE RESOLUTION MODEL OF THE LEEUWIN CURRENT SYSTEM

by

Scott Boedeker

December 2001

Thesis Advisor: Mary L. Batteen
Second Reader: Robert H. Bourke

Approved for public release; distribution is unlimited.

Report Documentation Page

Report Date	Report Type	Dates Covered (from... to)
19 Dec 2001	N/A	-

Title and Subtitle A Fine Resolution Model of the Leeuwin Current System	**Contract Number**
	Grant Number
	Program Element Number
Author(s) Scott Boedeker	**Project Number**
	Task Number
	Work Unit Number
Performing Organization Name(s) and Address(es) Naval Postgraduate School Monterey, California	**Performing Organization Report Number**
Sponsoring/Monitoring Agency Name(s) and Address(es)	**Sponsor/Monitor's Acronym(s)**
	Sponsor/Monitor's Report Number(s)
Distribution/Availability Statement Approved for public release, distribution unlimited	
Supplementary Notes	
Abstract	
Subject Terms	
Report Classification unclassified	**Classification of this page** unclassified
Classification of Abstract unclassified	**Limitation of Abstract** UU
Number of Pages 76	

REPORT DOCUMENTATION PAGE

Form Approved OMB No. 0704-0188

1. AGENCY USE ONLY *(Leave blank)*	2. REPORT DATE	3. REPORT TYPE AND DATES COVERED
	December 2001	Master's Thesis

4. TITLE AND SUBTITLE A Fine Resolution Model of the Leeuwin Current System

5. FUNDING NUMBERS

6. AUTHOR (S) LT Scott Boedeker

7. PERFORMING ORGANIZATION NAME(S) AND ADDRESS(ES)
Naval Postgraduate School
Monterey, CA 93943-5000

8. PERFORMING ORGANIZATION REPORT NUMBER

9. SPONSORING / MONITORING AGENCY NAME(S) AND ADDRESS(ES)

10. SPONSORING/MONITORING AGENCY REPORT NUMBER

11. SUPPLEMENTARY NOTES The views expressed in this thesis are those of the author and do not reflect the official policy or position of the U.S. Department of Defense or the U.S. Government.

12a. DISTRIBUTION / AVAILABILITY STATEMENT
Approved for public release; distribution is unlimited

12b. DISTRIBUTION CODE

13. ABSTRACT ***(maximum 200 words)***

To investigate the role of wind forcing, bottom topography and thermohaline gradients on classical as well as unique features of the Leeuwin Current system (LCS), five experiments are conducted with a sigma coordinate, primitive equation model on a beta-plane. The first experiment, which investigates the pressure gradient force error, shows that velocity errors, inherent in three dimensional sigma coordinate models, can be successfully reduced from ~100 cm/s to ~1 cm/s in the LCS. The second experiment, which highlights the effect of annual wind forcing on a flat bottom with horizontally averaged climatology, portrays some classical features of eastern boundary currents such as an equatorward surface current and upwelling. The third experiment uses horizontally averaged climatology and annual winds, but adds realistic topography to investigate its role in the LCS. This results in a different upwelling pattern and a poleward surface current inshore of the main equatorward current. The fourth experiment uses annual temperature and salinity values to investigate the effects of the thermohaline gradient without the annual wind over topography. The addition of the thermohaline gradient drives a strong poleward (equatorward) surface current (undercurrent). The final experiment attempts to model the LCS using full climatology and annual winds over realistic topography. The results show that despite equatorward winds, the thermohaline gradient continues to force a surface poleward current (equatorward undercurrent).

14. SUBJECT TERMS	15. NUMBER OF PAGES
Primitive equation model, Leeuwin Current, sigma level, Princeton Ocean Model (POM)	76
	16. PRICE CODE

17. SECURITY CLASSIFICATION OF REPORT	18. SECURITY CLASSIFICATION OF THIS PAGE	19. SECURITY CLASSIFICATION OF ABSTRACT	20. LIMITATION OF ABSTRACT
Unclassified	Unclassified	Unclassified	UL

NSN 7540-01-280-5500 **Standard Form 298 (Rev. 2-89)**
Prescribed by ANSI Std. 239-18

THIS PAGE INTENTIONALLY LEFT BLANK

A FINE RESOLUTION MODEL OF THE LEEUWIN CURRENT SYSTEM

Scott Boedeker
Lieutenant, United States Navy
B.S., United States Naval Academy, 1993

Submitted in partial fulfillment of the
requirements for the degree of

MASTER OF SCIENCE IN METEOROLOGY AND PHYSICAL OCEANOGRAPHY

from the

NAVAL POSTGRADUATE SCHOOL
December 2001

Author: _____
Scott Boedeker

Approved by: _____
Mary L. Batteen, Thesis Advisor

_____
Robert H. Bourke, Second Reader

_____
Mary L. Batteen, Chairman
Department of Oceanography

THIS PAGE INTENTIONALLY LEFT BLANK

ABSTRACT

To investigate the role of wind forcing, bottom topography and thermohaline gradients on classical as well as unique features of the Leeuwin Current system (LCS), five experiments are conducted with a sigma coordinate, primitive equation model on a beta-plane. The first experiment, which investigates the pressure gradient force error, shows that velocity errors, inherent in three dimensional sigma coordinate models, can be successfully reduced from ~100 cm/s to ~1 cm/s in the LCS. The second experiment, which highlights the effect of annual wind forcing on a flat bottom with horizontally averaged climatology, portrays some classical features of eastern boundary currents such as an equatorward surface current and upwelling. The third experiment uses horizontally averaged climatology and annual winds, but adds realistic topography to investigate its role in the LCS. This results in a different upwelling pattern and a poleward surface current inshore of the main equatorward current. The fourth experiment uses annual temperature and salinity values to investigate the effects of the thermohaline gradient without the annual wind over topography. The addition of the thermohaline gradient drives a strong poleward (equatorward) surface current (undercurrent). The final experiment attempts to model the LCS using full climatology and annual winds over realistic topography. The results show that despite equatorward winds, the thermohaline gradient continues to force a surface poleward current (equatorward undercurrent).

THIS PAGE INTENTIONALLY LEFT BLANK

TABLE OF CONTENTS

THIS PAGE INTENTIONALLY LEFT BLANK

LIST OF FIGURES

THIS PAGE INTENTIONALLY LEFT BLANK

LIST OF TABLES

THIS PAGE INTENTIONALLY LEFT BLANK

ACKNOWLEDGEMENTS

I would like to thank Prof. Mary Batteen for all of the time she has committed in helping me complete this thesis. Her help, knowledge and guidance throughout the process has been immense. Thank you. I would also like to thank Prof. Robert Bourke for his thoughtful input and advice as my second reader. Muito obrigado to Antonio Martinho for the hours of assistance he has given. His computer expertise made this project possible. Thanks also to my wife, Melissa, for all of her support. For anyone who may read this, Fly Navy!

THIS PAGE INTENTIONALLY LEFT BLANK

I. INTRODUCTION

The Leeuwin Current is a thermally driven, anomalous, surface eastern boundary current (EBC). It flows poleward over the continental shelf break (~200 m) off the coast of western Australia to Cape Leeuwin (see Figure 1) and then eastward into the Great Australian Bight (Cresswell and Golding, 1980). There is general agreement (Godfrey and Ridgway, 1985) that the Leeuwin Current is generated by a meridional pressure gradient resulting from the large amount of heating in the equatorial region and excessive cooling near the poleward region that overwhelms the equatorward wind stress. The source for the Leeuwin Current is predominantly an alongshore steric height gradient due to tropical Pacific water from the Indonesian throughflow (Godfrey and Ridgway, 1985, Hirst and Godfrey, 1993), augmented by geostrophic inflow from the west (McCreary et al., 1986; Thompson, 1987). As a result of this strong inflow of subtropical water towards the coast, the Leeuwin Current intensifies poleward (Batteen et al., 1992). The Leeuwin Current flows most predominantly but not exclusively in the austral autumn and winter (Church et al., 1989). The surface poleward current along the Australian west coast is weakest and shallowest between November and January when the equatorward wind stress is at a maximum, with the period of strongest and deepest flow between March and May when the equatorward wind stress is at a minimum.

The Leeuwin Current is unlike other subtropical EBCs. The major subtropical EBCs such as the California, Canary,

Peru, and Benguela Currents are wind-driven and characterized by climatologically weak (<10 cm/s), broad (~1000 km wide), cold surface flows towards the equator in the direction of the prevailing winds; a poleward undercurrent; a shallow (<30 m depth) thermocline and high biological production due to vast regional upwelling (Parrish et al., 1983). Observational studies along the coast of western Australia have shown that the Leeuwin Current is characterized by a strong (>150 cm/s at times), narrow (<100 km wide), poleward surface current that flows opposite the prevailing wind direction (Cresswell and Golding, 1980; Godfrey et al., 1986), anomalous warm water at the surface, a deep (>50 m depth) thermocline (Thompson, 1984), and lower biological production due to vast regions of downwelling (Batteen et al., 1992).

Below the Leeuwin Current, an anomalous equatorward undercurrent is present off western Australia (Church et al., 1989). Smith et al. (1991) stated that the speed of the undercurrent can reach ~30 cm/s between ~250 m and 350 m and observed that current meter data from the LUCIE experiment showed the equatorward current to be narrow and confined to the continental shelf slope between ~250 m and 450 m. Although there is evidence of a westward flow of ~20 cm/s centered between ~400 m and 700 m depth off the southern coast at ~116° E (Cresswell and Peterson, 1993), no studies to date have clearly resolved whether the existence of a westward undercurrent in this region.

Previous numerical modeling studies by Batteen et al. (1992) investigated the effects of annual climatological wind forcing and initialized thermohaline gradients on the

Leeuwin Current System (LCS), but the study was limited to the coast off western Australia and did not include the influence of topography. Batteen and Butler (1998) examined the effects of continuously forced annual Indian Ocean thermohaline gradients on the LCS and extended the domain to include both the western and southwestern coasts of Australia. Tworek (2000) investigated the effects of seasonal forcing on the LCS with a full primitive equation ocean model but again only considered flat bottom cases.

This study seeks to extend prior efforts in this area by including the addition of realistic topography, allowing a better understanding of the LCS by including the influences of topography. The Princeton Ocean Model (POM), a bottom-following sigma coordinate model, was chosen for this study because it has been widely used to simulate coastal processes associated with continental shelf flows and bottom boundary layer dynamics. The results of several numerical experiments (Table 1) are explored. Each experiment includes the effects of thermohaline forcing at the four open boundaries on a beta plane. In Experiment 1 velocity errors produced by the pressure gradient force error, an error inherent in all three-dimensional sigma coordinate models, are determined using horizontally averaged annual climatology with bottom topography and no wind forcing. In Experiment 2 the horizontally averaged annual climatology is used with annual wind forcing on a flat bottom. Experiment 3 repeats Experiment 2 but with the addition of bottom topography. To explore the roles of wind and bottom topography on the LCS, the results of Experiments 2 and 3 are compared to each other. These two experiments are more typical of EBC regions other than the

LCS; they are presented to highlight the wind field forcing without the thermohaline gradient. The final two experiments are more representative of the LCS due to inclusion of the annual climatology. Experiment 4 shows the effects of thermohaline forcing over topography without wind forcing. Experiment 5 is the most complete and accurate representation of the LCS. This final experiment incorporates realistic bottom topography with the annual wind and thermohaline forcing from Experiment 4.

This study is organized as follows. In section II we describe the numerical model and the specific experimental conditions. The results of the numerical experiments are presented in section III. A summary is presented in section IV.

II. MODEL DESCRIPTION

A. DATA SETS

The topographic data of the study region was obtained from the Institute of Geophysics and Planetary Physics, University of California San Diego (Sandwell and Smith, 1996). The data set has a resolution of 2 minutes (1/30 of a degree) based upon a 30-year compilation of bottom echo soundings by ships. Where the ship data is sparse, altimetry information was used to interpolate soundings.

Annual temperature and salinity values were obtained from Levitus and Boyer (1994) and Levitus et al. (1994). These data sets incorporate a 1 by 1 degree horizontal resolution at the vertical levels shown in Table 2.

For wind forcing, climatological wind fields were obtained from the European Center for Medium Range Weather Forecasts (ECMWF) near-surface wind analyses (Trenberth et al., 1990). The wind data are formulated on a 2.5 by 2.5 degree grid.

All experiments were performed on a beta-plane with a realistic coastline.

B. PRE-PROCESSING

The original topography (Figures 2a and b) was interpolated with a Gaussian filter to the resolution used in the model, i.e., 10 km by 10 km offshore, 3 km by 10 km alongshore and 3 km by 3 km around the southwest corner of Australia, with a total of 252 by 226 points. The highest

resolution was positioned around the southwest corner of Australia with higher resolution in a north-south band overlapping an east-west band of higher resolution (Figure 3). This was done to minimize the slope parameter (defined by Mellor et al., 1998, as $\frac{|\delta H|}{2 * \overline{H}}$, where $\overline{H}$ is the average depth and δH is the difference in depth between two adjacent cells), which is greatest along the shelf. Since over much of the area the slope parameter was greater than 0.2, which is the suggested maximum value to be used in sigma coordinate models (Mellor et al., 1998), the topography was first smoothed with a 2D Gaussian filter. The new depth of each point calculated with this filter is a Gaussian-shaped, weighted average of 25 by 25 points with a standard deviation of 8. After initial smoothing, all depths greater than 2500 m were reassigned to a depth of 2500 m. Land was assigned a depth of 20 m (to avoid division by zero in the model). Any remaining areas that exceeded a slope parameter of 0.2 were manually filled to achieve an acceptable slope parameter. The new topography is shown in Figures 4a and 4b.

The annual temperature and salinity values were interpolated for the horizontal spatial resolution of the model and for the 21 vertical sigma levels (Table 3 and Figure 5) using a three-dimensional (3D) linear interpolation scheme. The interpolation had to be done separately for the smoothed topography and flat bottom experiments due to the change in vertical levels between these two topographies. The annual temperature and

salinity fields at the surface (sigma level one) are shown in Figures 6 and 7, respectively.

The daily seasonal winds were averaged over time in order to obtain the annual non-weighted average wind vector field (Figure 8). The wind vectors were interpolated for the horizontal spatial resolution of the model with a 2D linear interpolation scheme. The components of the wind stress were then calculated.

C. BRIEF MODEL DESCRIPTION

The Princeton Ocean Model, POM, a well documented model (e.g., Blumberg and Mellor, 1987; Mellor, 1996), was used in the model studies. POM is a primitive equation, free surface model with a second moment turbulence closure scheme (Mellor and Yamada, 1982) that, through the use of bottom-following sigma levels, can realistically simulate processes associated with continental shelf flows and bottom boundary layer dynamics in local domains (e.g., bays, estuaries and coastal regions). Recently, the model has been used successfully to simulate decadal processes in entire ocean basins (Ezer and Mellor, 1994,1997).

As described earlier, the resolution of the horizontal grid varies between a minimum of 3 km by 3 km and a maximum of 10 km by 10 km (Figure 3). The varying grid allows the use of more (fewer) points in regions of large (small) gradients.

The 21 sigma levels used are shown in Figure 5 and Table 3. The sigma values range from zero at the surface to minus one at the bottom with the vertical grid spacing

proportional to the ocean depth. The vertical resolution has been chosen to be higher near the surface and the bottom in order to resolve both the surface boundary layer (SBL) and the bottom boundary layer (BBL) which are important in coastal regions. To eliminate the time constraints for the vertical grid related to the higher resolution near the surface, bottom and shallow waters, an implicit vertical time differencing scheme was used.

The prognostic variables of the model are potential temperature, salinity, density, the three components of velocity, surface elevation, turbulent kinetic energy and length scale. The model uses a split time step for the external and internal modes. The external mode solves the equations for the vertically integrated momentum equations. It also provides the sea surface and barotropic velocity components, and has a time step of 4 seconds. The internal mode solves the complete 3D (baroclinic) equations and has a time step of 180 seconds.

A Smagorinsky formulation (Smagorinsky et al., 1965) is used for the horizontal diffusion in which the horizontal viscosity coefficients depend on the grid size, the velocity gradients and a coefficient. In this study a value of 0.2 was assigned to this coefficient, consistent with other POM studies (e.g., Ezer and Mellor, 1997).

D. INITIALIZATION, FORCING AND BOUNDARY CONDITIONS

The model was initialized with annual temperature and salinity values obtained from Levitus and Boyer (1994) and Levitus et al. (1994). Since the model runs reached a quasi-equilibrium state in a relatively short time (~60

days), zero salinity and temperature fluxes were prescribed at the ocean surface. The climatological surface temperature (Figure 6) shows a latitudinal decrease in temperature within the domain with the warmest water at each latitude near the coast. The climatological salinity (Figure 7) shows a maximum of ~38.9 psu at the center of the western edge of the model domain and minima in the north (~35.3 psu) at the coast and along the southern edge (~35.1 psu). The first three experiments use horizontally averaged values of annual temperature and salinity such that the surface temperature and salinity initialized over the entire domain are ~19.8°C and ~35.39 psu respectively.

The model was forced from rest with the annual ECMWF wind fields, which were interpolated for the model grid. As expected, the wind stress is westerly in the southern region of the model domain and south-southeasterly along the west coast. The SSE winds strengthen with latitude, away from Australia (Figure 8).

Correct specification of the open boundary conditions (BC) is important to achieve realistic results, with no reflections, clamping, spurious currents or numerical alteration of the total volume of water in the model. No general criterion is currently available that can provide the answer to what boundary conditions are the best for a specific model or study. For models with a free surface, such as used here, one of the important criterion is that the BCs should be transparent to the waves. In this model, a gradient boundary condition (Chapman, 1985) which allows geostrophic flow normal to the boundary worked best for the elevation. For the baroclinic velocity components normal

to the boundary, an explicit wave radiation scheme based on the Sommerfield radiation condition was used. For inflow situations, the model was forced with annual temperature and salinity values obtained from Levitus and Boyer (1994) and Levitus *et al*. (1994), while in outflow situations an advection scheme was used. A volume constraint was used to ensure the volume remained constant (Marchesiello et al., 2001).

For the barotropic velocity components, a Flather radiation plus Roed local solution (FRO) was used. Palma and Matano (2000) showed good results with the FRO solution during BC tests to determine the BCs response to an alongshelf wind stress. Palma and Matano (1998) also showed that the FRO BC demonstrated good reflection properties and results in a test that determined the BC response to the combined action of wind forcing and wave radiation. Their tests were executed with the barotropic version of POM and compared with benchmark results (no boundary conditions).

III. RESULTS FROM MODEL SIMULATIONS

A. PRESSURE GRADIENT FORCE ERROR DETERMINATION

In this first experiment, the model was initialized at rest with horizontally averaged annual climatological temperatures and salinities. A realistic coastline and bottom topography were used but no wind or thermohaline forcing was permitted.

With horizontally averaged climatology and no forcing mechanisms, we would expect that nothing will happen, i.e., the initial state of rest should be maintained. Due to pressure gradient force errors, however, this will not be the case and there will be velocities that result from these errors.

Velocity errors induced by the pressure gradient force are unavoidable in 3D sigma-coordinate models. Two types of sigma-coordinate errors exist, the sigma error of the first kind (SEFK) and of the second kind (SESK), as defined by Mellor et al. (1998). The first one goes to zero prognostically by advecting the density field to a new state of equilibrium. The second one, a vorticity error, is the most important because it does not vanish with time, and is present in both 2D and 3D cases.

There are several techniques to reduce the pressure gradient errors:

1. Smoothing the topography can reduce both SEFK and SESK. In particular, the slope parameter should not be greater than 0.2 (Mellor et al., 1998). Greater

values can artificially induce currents over 1 m/s.

2. Using the highest possible resolution can reduce the errors, since the pressure gradient error decreases with the square of the horizontal and vertical grid size.

3. Subtracting the horizontally averaged density before the computation of the baroclinic integral reduces the SESK.

4. Using a curvilinear grid that follows the bathymetry reduces the SESK.

This study used the first three techniques. The use of a curvilinear grid was not employed since the first three techniques successfully reduced the error to an acceptable level.

To show where the velocity errors are present in the model domain, the velocity field for day 60 at sigma level 1 (surface) is shown in Figure 9. As expected, maximum velocities of ~1 cm/s are found along the coast where the slope parameter is the greatest. These results are similar to those obtained by Martinho (2001) and indicate that with the use of the three error reduction techniques, the pressure gradient force error has been considerably reduced (~1 m/s).

B. WIND EFFECTS ON A FLAT BOTTOM

This experiment seeks to highlight the role of wind forcing alone in the Leeuwin Current System (LCS). Toward this end, the model was initialized with horizontally averaged annual climatological temperatures and salinities over a flat bottom. A realistic coastline was used and the model was forced with the annual climatological winds.

By day 20 (Figure 10a) the southeasterly winds along the west coast have caused weak upwelling as evidenced by the coldest water at the coast from Shark Bay in the north to near Perth in the south. A weak equatorward current has developed off Perth. The offshore upwelling and westward current in the northeast corner of the domain is likely due to speed divergence in the annual wind field as it accelerates away from the coast. The water temperature at the coast has decreased about 0.5°C from the initial value.

At day 40 (Figure 10b) the coastal upwelling continues to increase north of 31°S, although it remains near the coast with little offshore extent. The weak equatorward current present off the coast near Perth remains ~10 cm/s.

By day 60 (Figure 10c) the coastal current has increased to ~40 cm/s and is now evident continuously from the eastern boundary, around the southwest corner, and up the coast to the northern boundary of the model domain. A typical cross-section (Figure 10d) taken at 34.3°S (westward off Cape Leeuwin) depicts the north-south velocity of the coastal current as well as a deep (1200-1700 m) poleward undercurrent. The undercurrent is broader (~100 km) and weaker (~20 cm/s) than the surface current.

C. WIND EFFECTS OVER TOPOGRAPHY

To isolate the effect of the wind field from thermohaline effects, the model was again initialized with horizontally averaged annual climatological temperatures and salinities. The same coastline and annual climatological winds were used; however, the local topography was introduced instead of a flat bottom.

By day 20 (Figure 11a) coastal upwelling has developed as in the previous case but it is not as strong. It is also apparent that the upwelling is less widespread than in the flat bottom case. There is also a weak equatorward current off Perth of ~10 cm/s as well as the area of likely speed divergence creating some offshore upwelling in the northwest.

At day 40 (Figure 11b) the upwelling, while less extensive, now appears to be just as cold with the coldest water in both cases ~19°C. Little upwelling is noted at 28°S in this experiment; but with the flat bottom, this area experienced some of the strongest upwelling. No upwelling is observed south of about 32°S and it remains localized in two areas north and south of 28°S.

By day 60 (Figure 11c), while the upwelling remains localized, (centered in the two areas around 27°S and 29°S), the equatorward current has moved farther offshore and strengthened to a maximum of ~80 cm/s at the surface. Inshore of the main current, a weaker (~20 cm/s) poleward current has formed and is evident down to 30°S. It is visible in the cross-section from 29°S (Figure 11d) where

one would expect the Leeuwin Current to be visible (above the 200 m isobath) but not in the cross-section from Cape Leeuwin (34.3°S) (Figure 11e). This poleward current is likely forced by shear in the annual wind field as the wind increases seaward in the cross-shore direction.

The addition of topography appears to hinder upwelling even with upwelling favorable winds. It also allows the creation of a poleward current trapped against the coast, even without a pressure gradient to force it. The results from experiments 2 and 3 are typical for EBC regions other than the LCS.

D. THERMOHALINE FORCING OVER TOPOGRAPHY

This experiment is initialized with full annual climatology but without wind forcing. It uses the same coastline and is run over the local topography. It introduces conditions unique to the LCS.

By day 20 (Figure 12a) a poleward coastal current has developed with a maximum velocity of ~80 cm/s. It is evident from the northern edge of the domain around the southwest corner of Australia to the eastern edge. This current advects warm water south with temperatures off Cape Leeuwin approaching 23°C. In addition to the coastal current, there is also a broad movement of offshore water to the south.

By day 40 (Figure 12b) the coastal current remains strong at ~80 cm/s. It continues to advect warm water poleward, with temperatures off Cape Leeuwin reaching 25°C. Several eddies have also begun to spin up; a dipole pair is

evident southwest of Cape Leeuwin. The broad movement of offshore water to the south is no longer evident.

By day 60 (Figure 12c) the current has increased beyond 1 m/s off Perth and Cape Leeuwin (Figure 12f) and continues to flow from the northern boundary to the eastern edge of the domain. The eddies appear to migrate seaward but the current is held against the coast. The cross-section westward from Cape Leeuwin (Figure 12d) shows the poleward surface current to be above the shelf-break (~200 m), where the Leeuwin Current would be expected to flow.

This experiment demonstrates that the unique climatological thermohaline gradient, over the topography of the region, drives a strong poleward current. Eddies develop but the topography keeps the current trapped near the coast.

E. WIND AND THERMOHALINE FORCING OVER TOPOGRAPHY

This experiment is the closest to simulating the LCS in the annual sense. The model was initialized with full annual temperature and salinity climatology over realistic bottom topography, as did the previous experiment. To this is added the annual wind forcing to build a complete, annual model of the LCS.

By day 20, (Figure 13a) a poleward warm current has formed along the coast with speeds to ~80 cm/s, very much like the no wind case. This current is evident along the entire coast of Australia bringing warmer temperatures farther south, faster.

By day 40 (Figure 13b) the warmest water is found at the coast with >23°C water along the entire coastline and above 25°C at Cape Leeuwin. Eddies develop along the coast but the current continues to be poleward.

By day 60 (Figure 13c), the Leeuwin Current remains strong, carrying warm, fresh water south and east along the Australian coast despite the many eddies that have formed along the coast. Many eddies have spawned; two dipole pairs are evident southwest of Cape Leeuwin. The cross-sections (Figures 13d, 13e, 13f) show the equatorward undercurrent intensifying over time between ~250-500 m depth, and the poleward Leeuwin Current above the 200 m contour.

This final and most complete experiment depicts a realistic LCS and highlights the important role played by the local topography. With the thermohaline gradient and topography used in the model, the warm water is trapped against the coast and the Leeuwin Current is maintained despite the adverse winds. The results are nearly identical to experiment 4 with slightly slower current speeds and greater eddy development. This indicates that the thermohaline gradient plays a dominant role in driving the Leeuwin Current. This differs from most other EBC regions, which are primarily wind driven.

THIS PAGE INTENTIONALLY LEFT BLANK

IV. SUMMARY

The objective of this study was to investigate the roles of wind forcing, thermohaline gradients, and particularly, topography in the Leeuwin Current System. Toward this end, five numerical experiments were run, all on a beta-plane, with a sigma coordinate numerical model, i.e., the Princeton Ocean Model. The first experiment determined the pressure gradient error. The second experiment investigated the effect of annual wind forcing over a flat bottom. The third experiment investigated the additional effect of topography. The fourth experiment investigated the role of the full, annual climatology over topography without annual wind forcing. The final experiment was run with full annual climatology and wind forcing over topography.

Experiment 1, used to evaluate the pressure gradient error, showed that the velocity errors inherent in sigma coordinate models could be reduced from ~1 m/s to ~.02 m/s using three techniques. The techniques used were: 1) smoothing the topography, 2) using the highest possible resolution, and 3) subtracting the area-averaged density before computation of the baroclinic integral. The results showed that the highest velocities (~2 cm/s) were along the coast where the values of the slope parameter were greatest.

Experiment 2 showed that the annual wind field, without a thermohaline gradient or topography forced an

equatorward surface current. It also produced extensive upwelling and a poleward undercurrent.

Experiment 3 added the local topography to the annual wind and horizontally averaged climatology used in experiment 2. This had the effect of limiting the extent of upwelling areas as well as the intensity of the upwelling. The addition of topography also trapped a poleward surface current inshore of the more dominate equatorward surface current. The results of experiments 2 and 3 are consistent with other EBC regions, but are uncharacteristic of the LCS.

Experiment 4 removed the wind forcing but introduced the annual climatological thermohaline gradient. Without the annual wind forcing, the effects of the thermohaline gradient over the topography are isolated. Thermohaline forcing is the dominant forcing mechanism in the LCS and it is shown to develop a strong, poleward surface current, eddies, and an equatorward undercurrent in this experiment. These features are all characteristics of the LCS.

Experiment 5 brings together the annual wind, annual climatology, and topography to most accurately represent the LCS in the annual sense. The results from experiment 5 differ from experiment four primarily in the maximum current speed and the eddy field. The wind, which opposes the thermohaline gradient, slows the poleward surface current slightly and enhances eddy spin-up.

The results of experiments 4 and 5 show that, in the annual sense, the wind is an almost insignificant factor compared to the thermohaline gradient. It is the seasonality of the wind, however, that determines when the

Leeuwin Current flows. Further research using seasonal winds and seasonal thermohaline forcing is recommended due to the seasonal nature of the observed Leeuwin Current.

THIS PAGE INTENTIONALLY LEFT BLANK

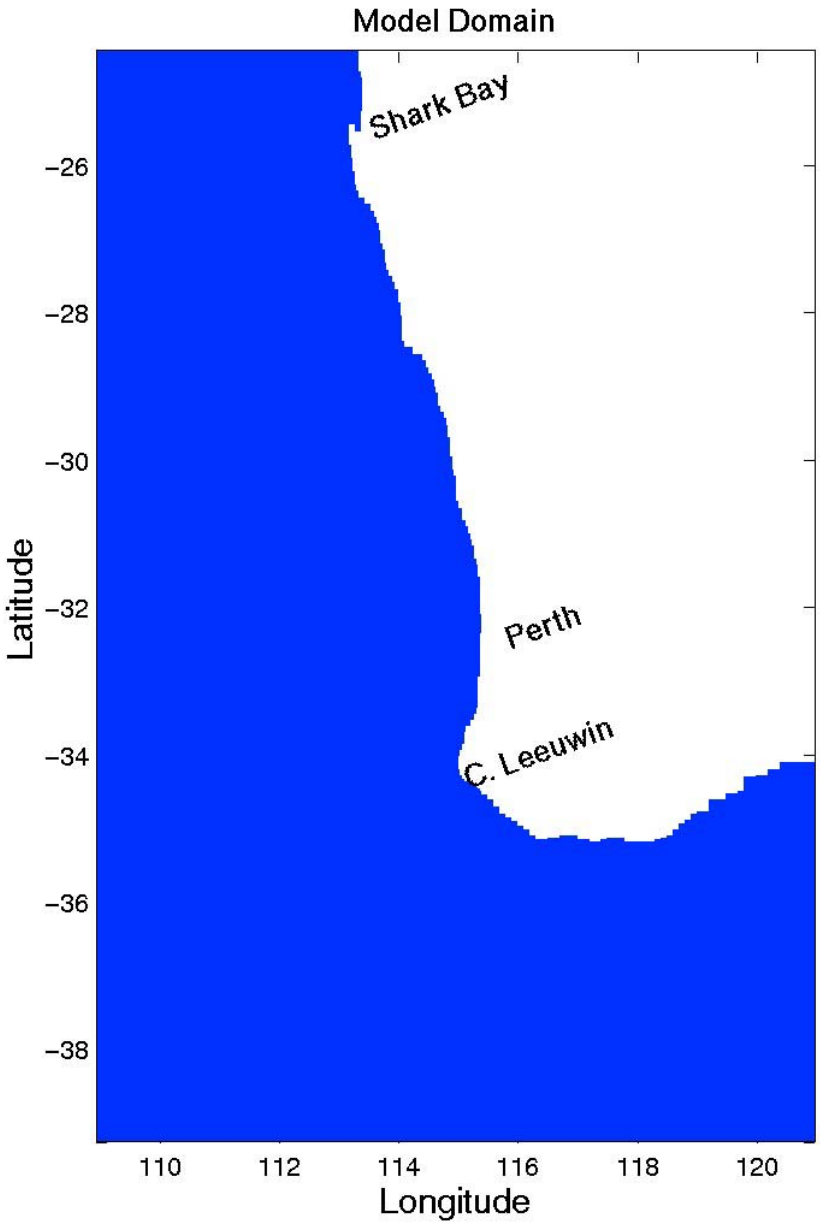

Figure 1. The model domain for the Leeuwin Current System (LCS) is bounded by 39°S to 24°S, 109°E to 121°E. The model domain has a closed boundary along the entire coast and four open boundaries.

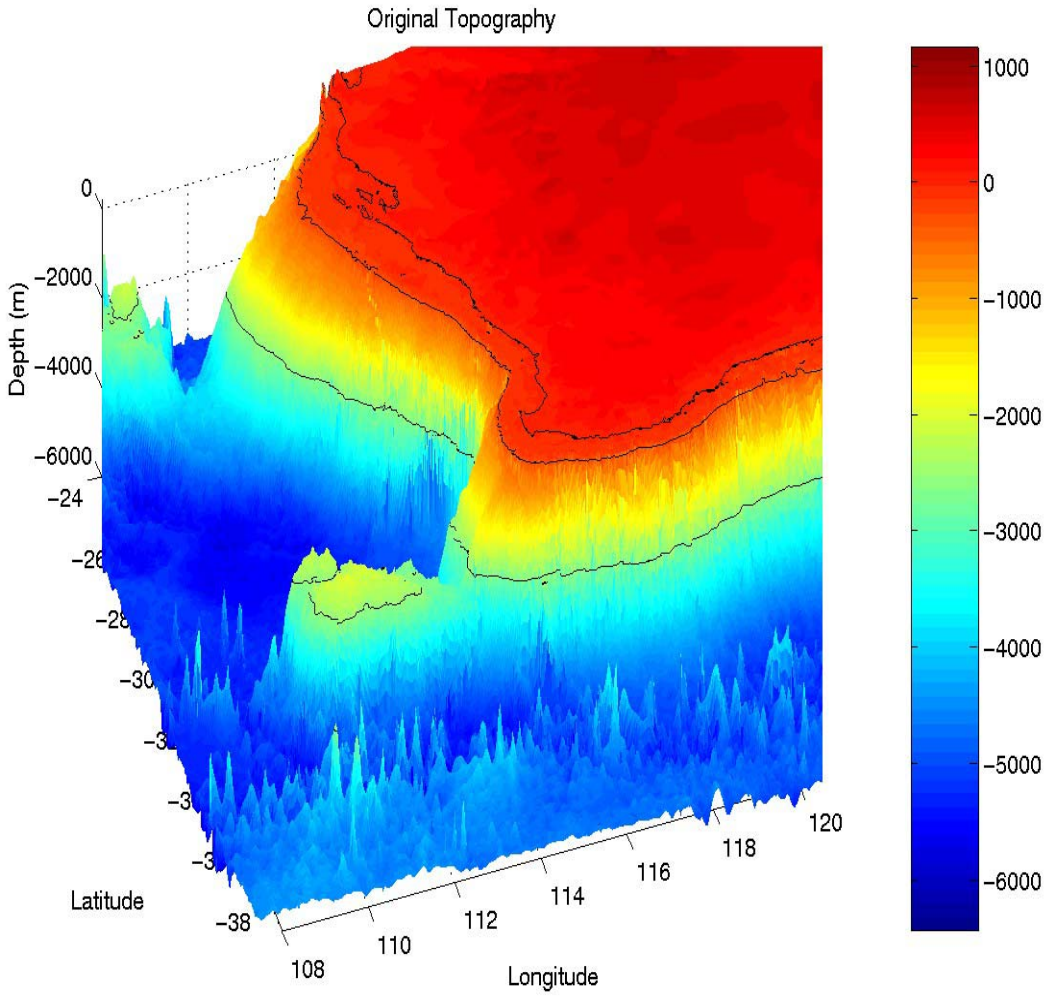

Figure 2a. Original topography in meters (from Sandwell and Smith, 1996) with a resolution of 2 minutes (1/30 degree). Contours depict the shoreline, 200m and 2500m isobaths.

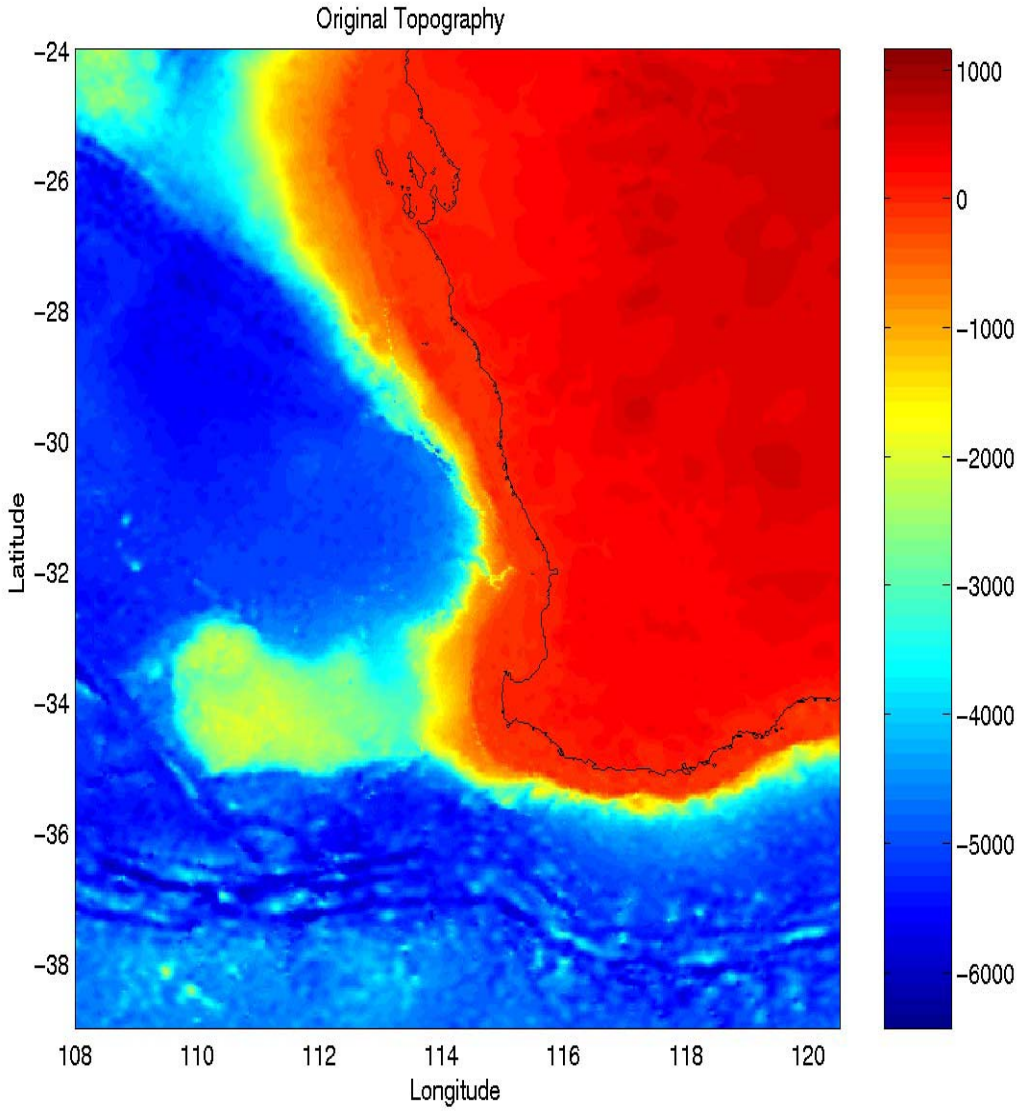

Figure 2b. Original topography (meters) in 2-D (from Sandwell and Smith, 1996) with a resolution of 2 minutes (1/30 degree).

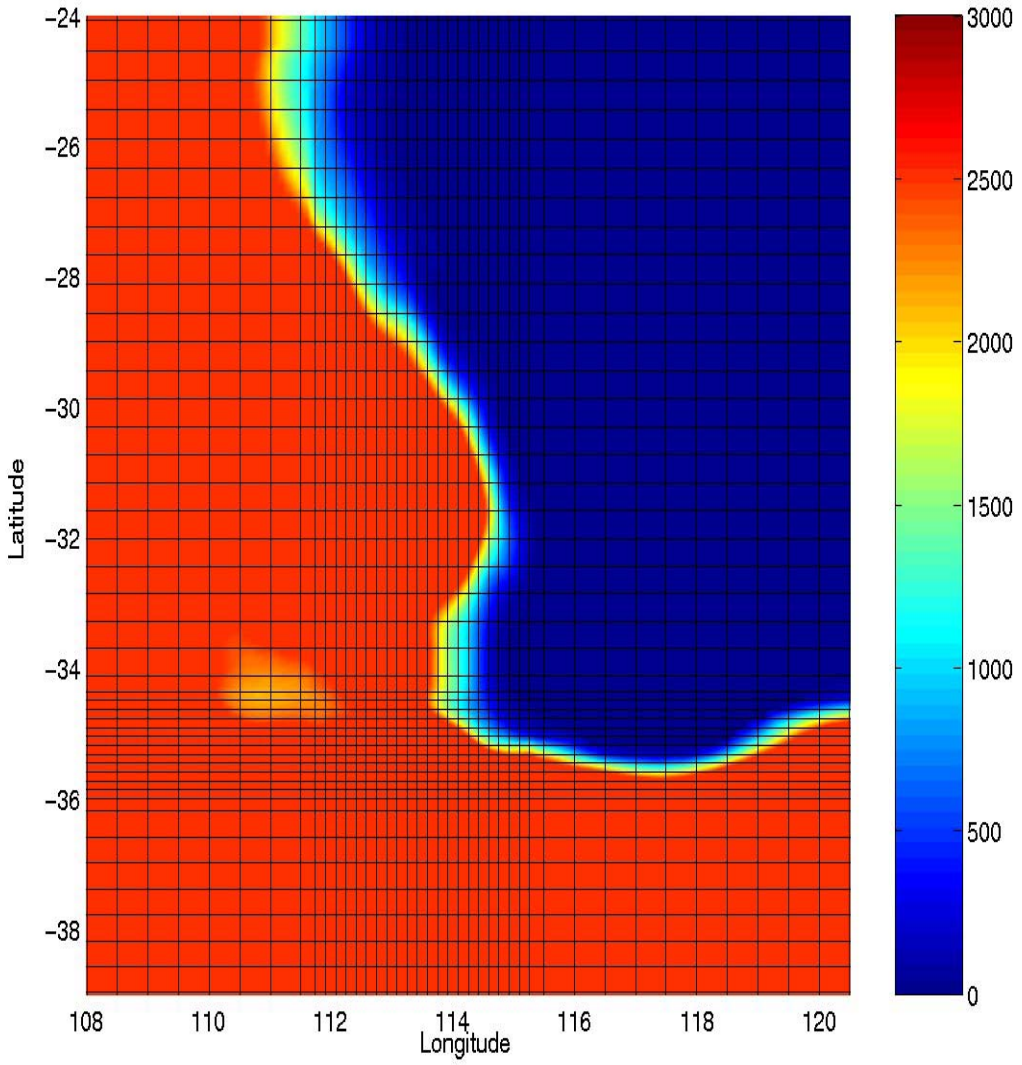

Figure 3. Resolution grid lines with every fifth grid line plotted. (10 by 10 km res. with two bands of 10 by 3 km and 3 by 10 km resolution)

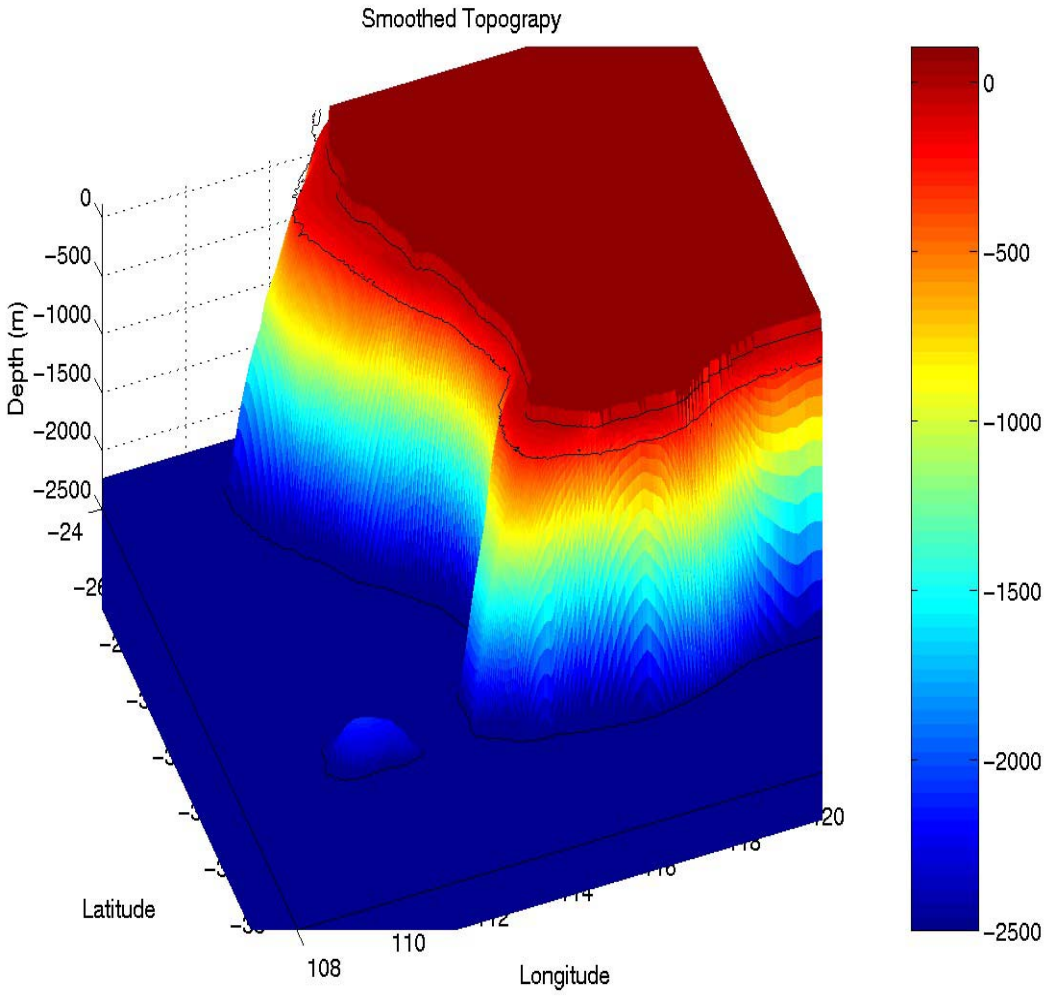

Figure 4a. Smoothed topography (meters) obtained after applying a two-dimensional Gaussian filter and reassigning depths greater than 2500 m to 2500 m. Contours depict the shoreline, 200 m and 2500 m isobaths.

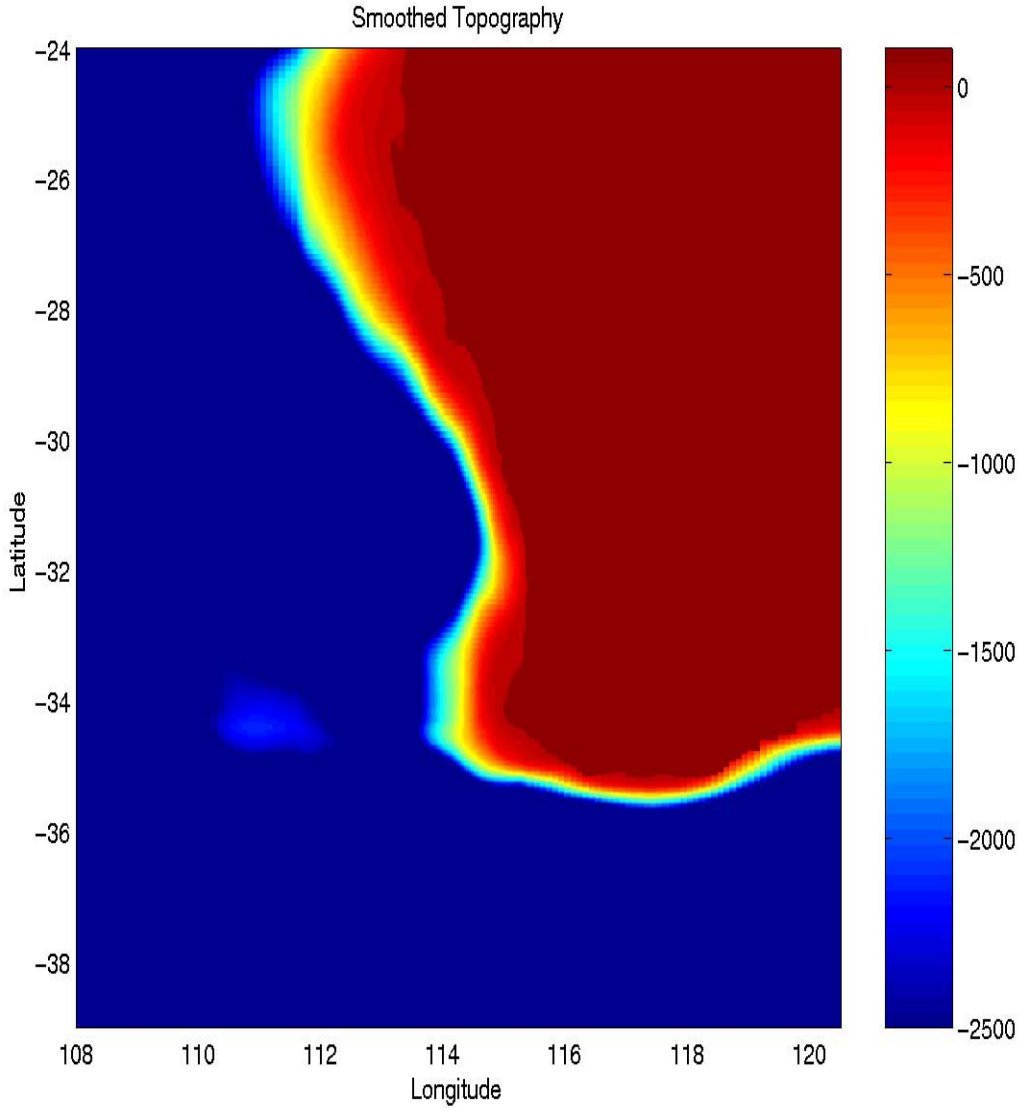

Figure 4b. Smoothed topography (meters) in 2-D obtained after applying a two-dimensional Gaussian filter and reassigning depths greater than 2500 m to 2500 m.

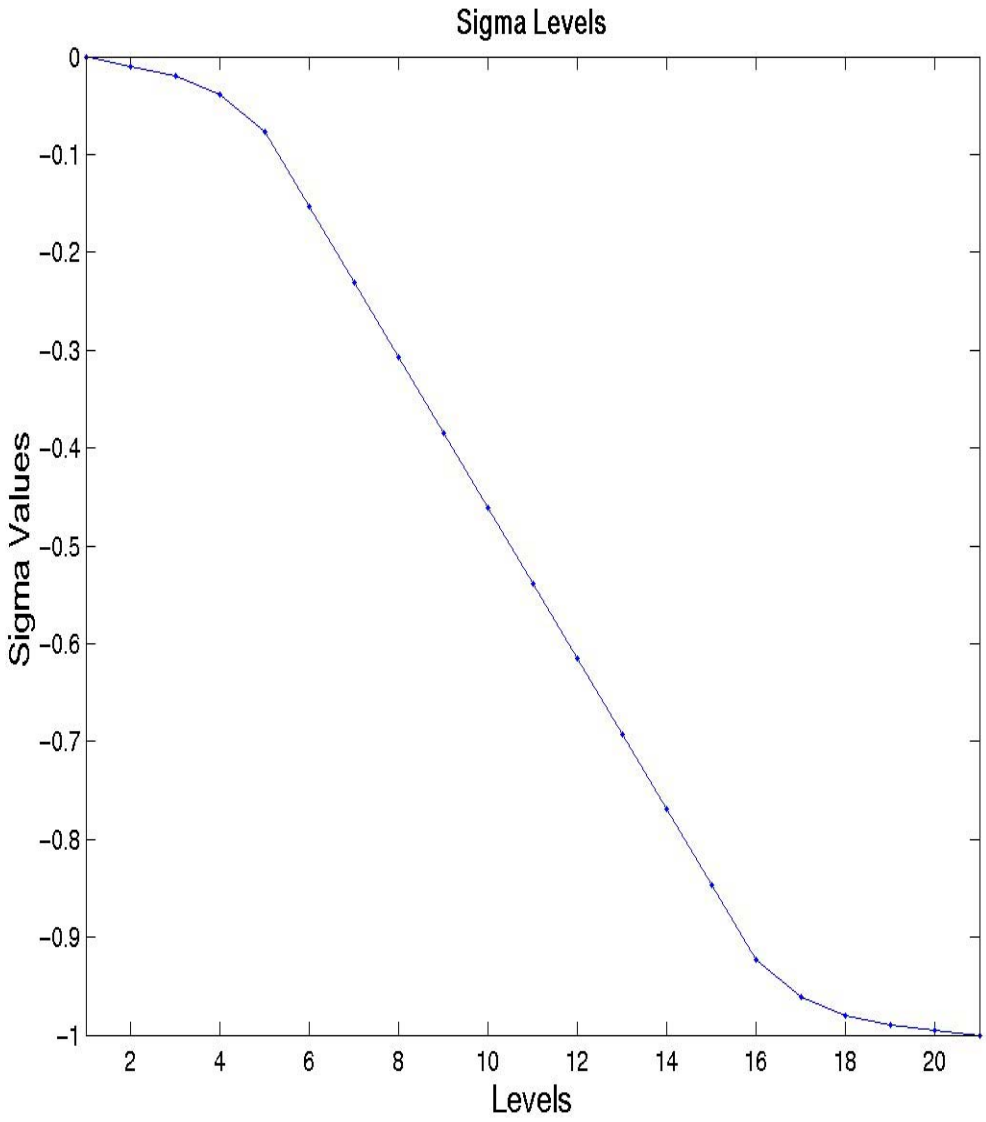

Figure 5. Plot of the 21 sigma levels.

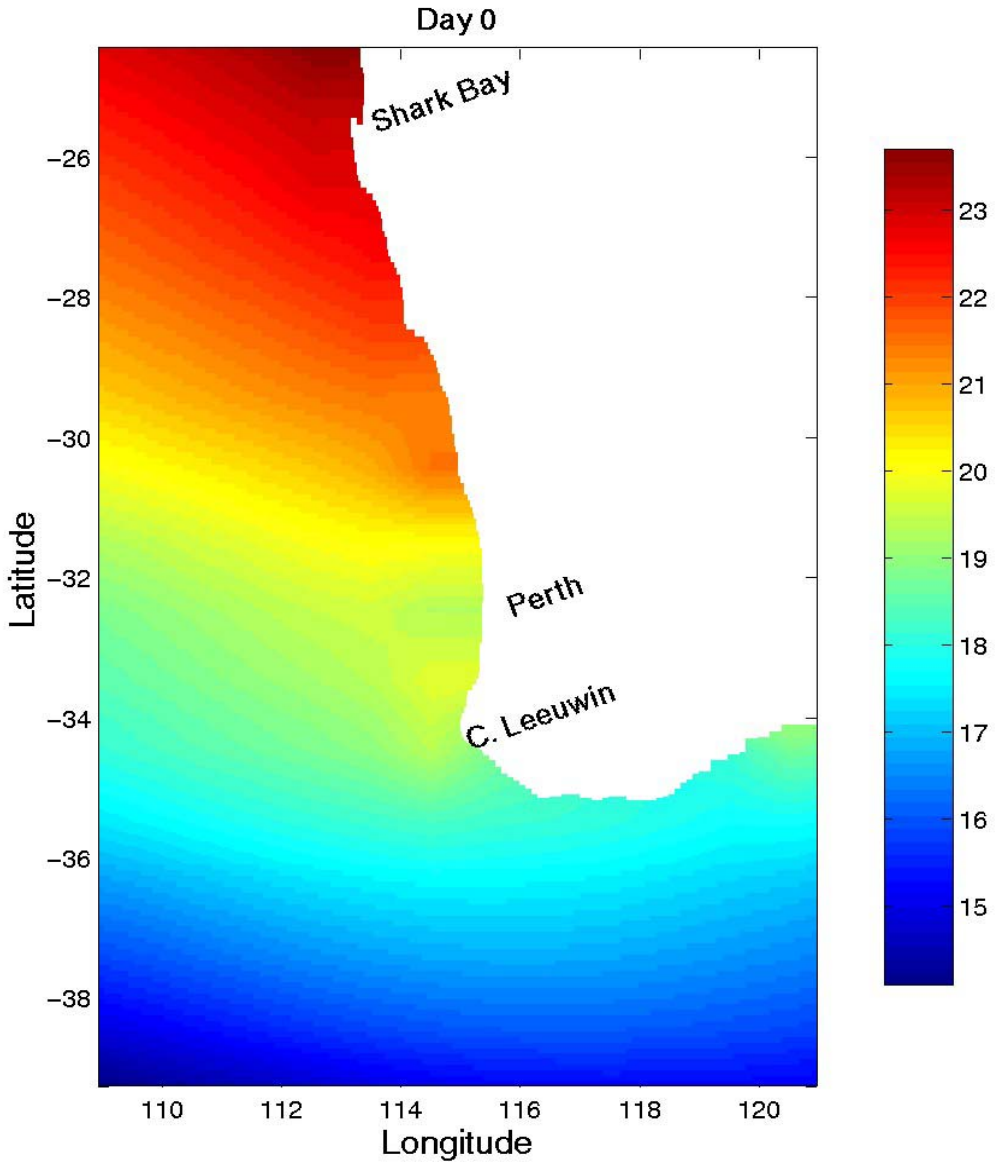

Figure 6. Annual climatological surface temperature (°C) from Levitus and Boyer, 1994.

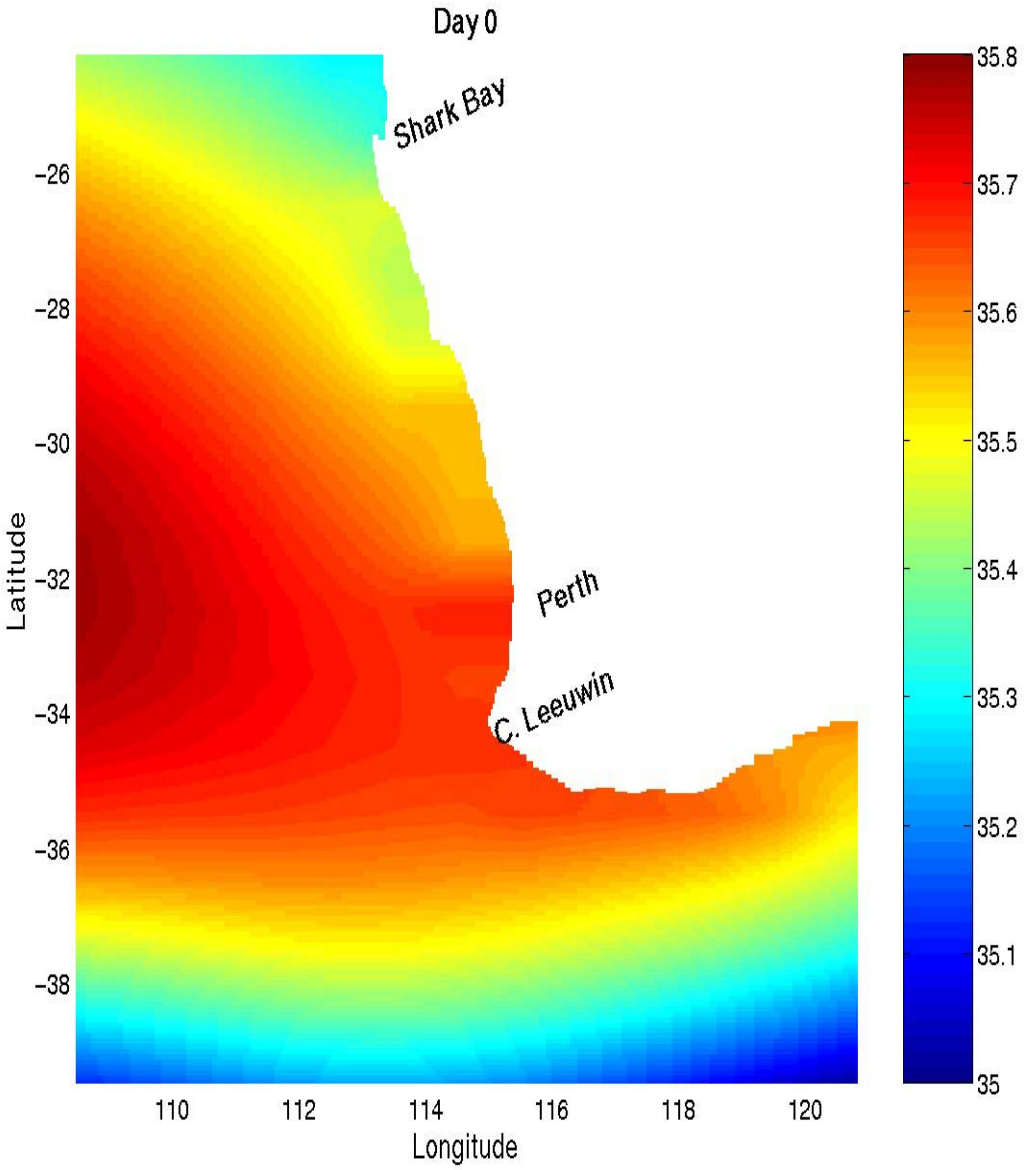

Figure 7. Annual climatological surface salinity (psu) from Levitus et al., 1994.

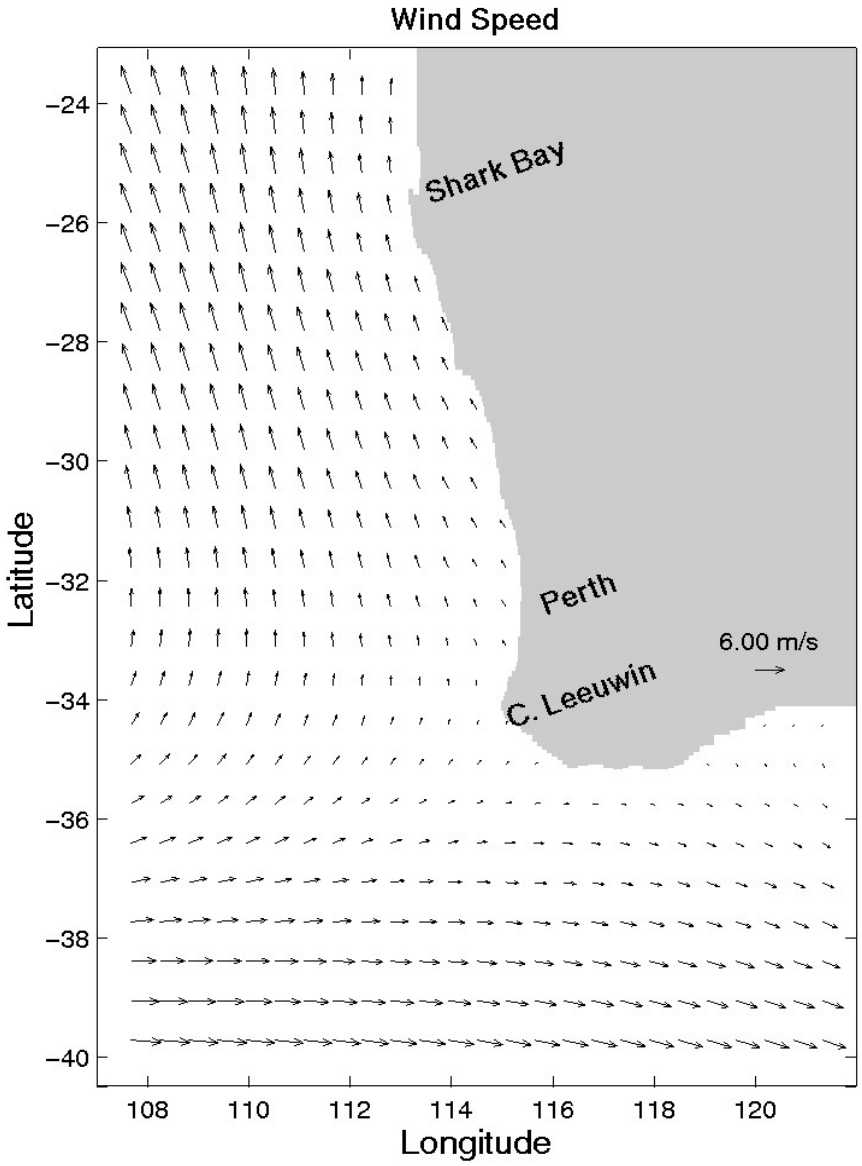

Figure 8. Annual average wind in m/s from climatological ECMWF winds obtained from Trenberth et al., 1990.

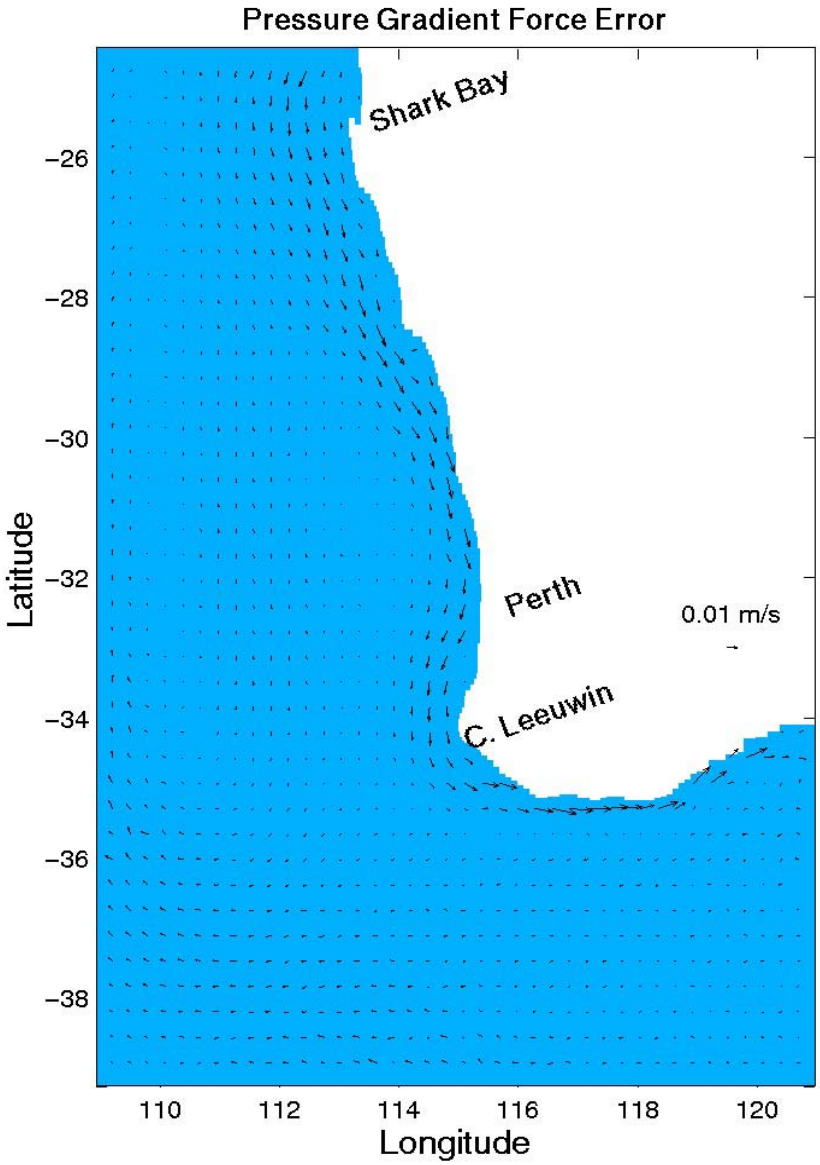

Figure 9. Surface velocity error (m/s) due to the pressure gradient force error on day 60 for Experiment 1.

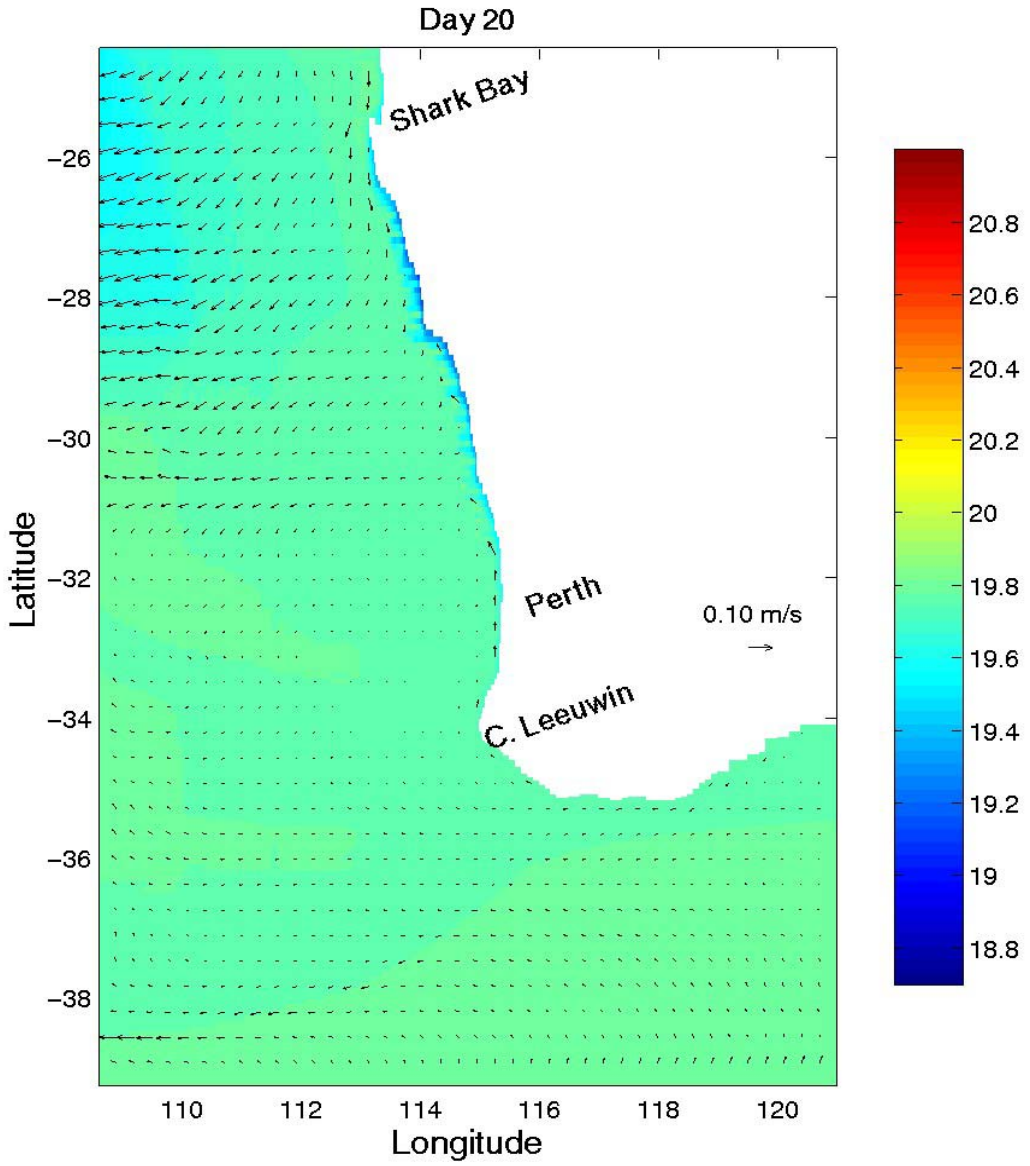

Figure 10a. Surface temperatures (°C) and velocity vectors for Experiment 2 on day 20.

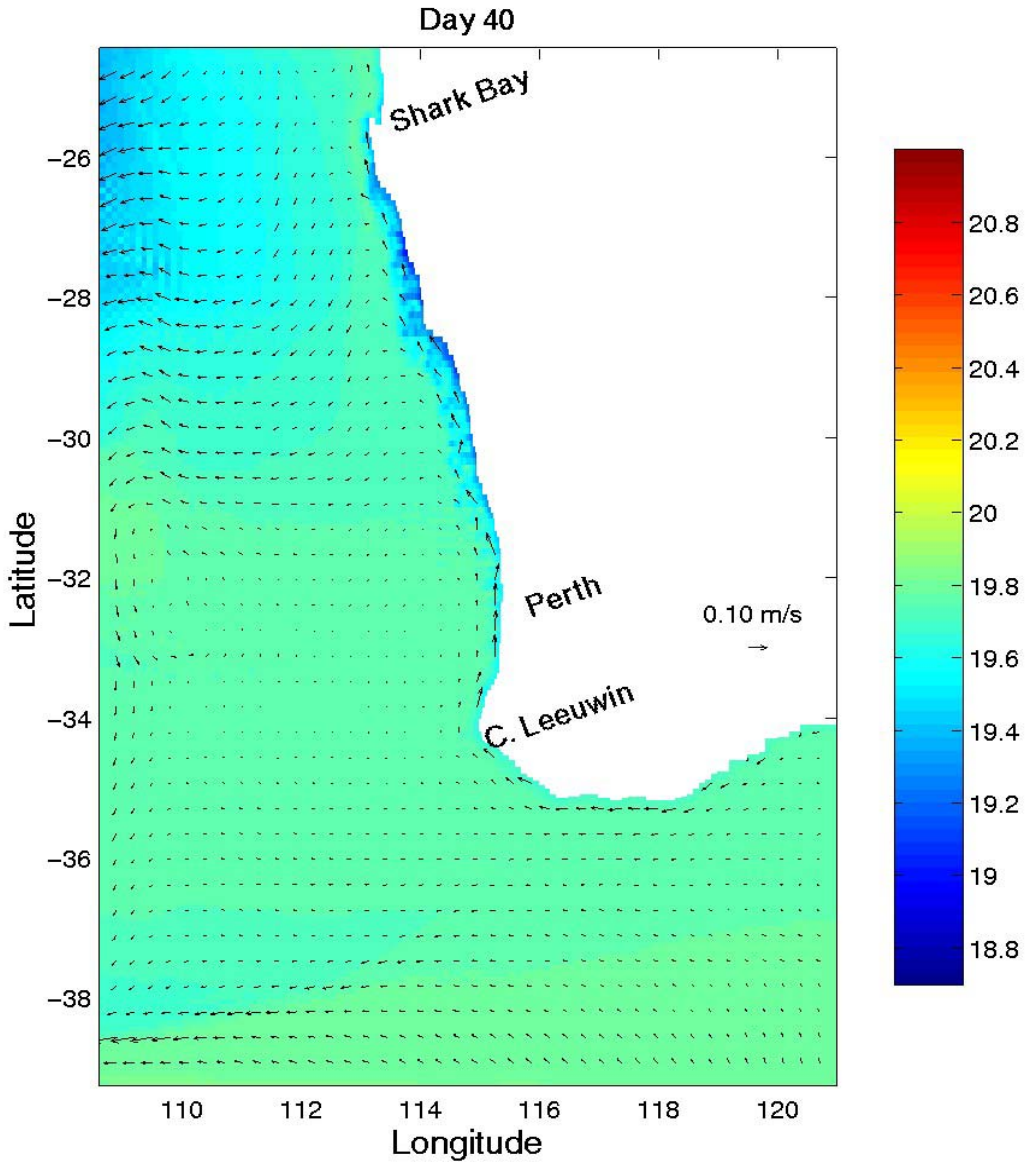

Figure 10b. Surface temperatures (°C) and velocity vectors for Experiment 2 on day 40.

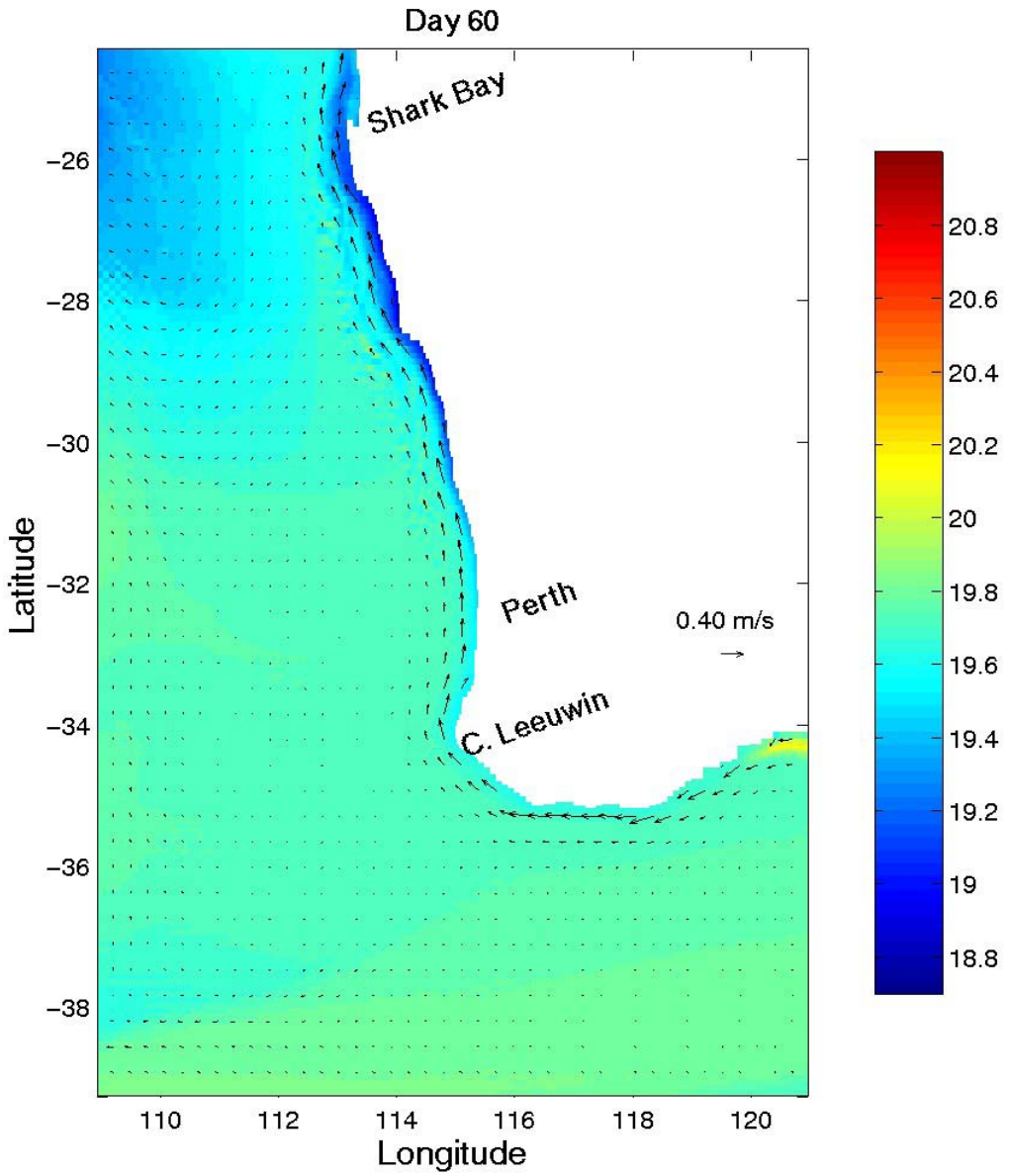

Figure 10c. Surface temperatures (°C) and velocity vectors for Experiment 2 on day 60.

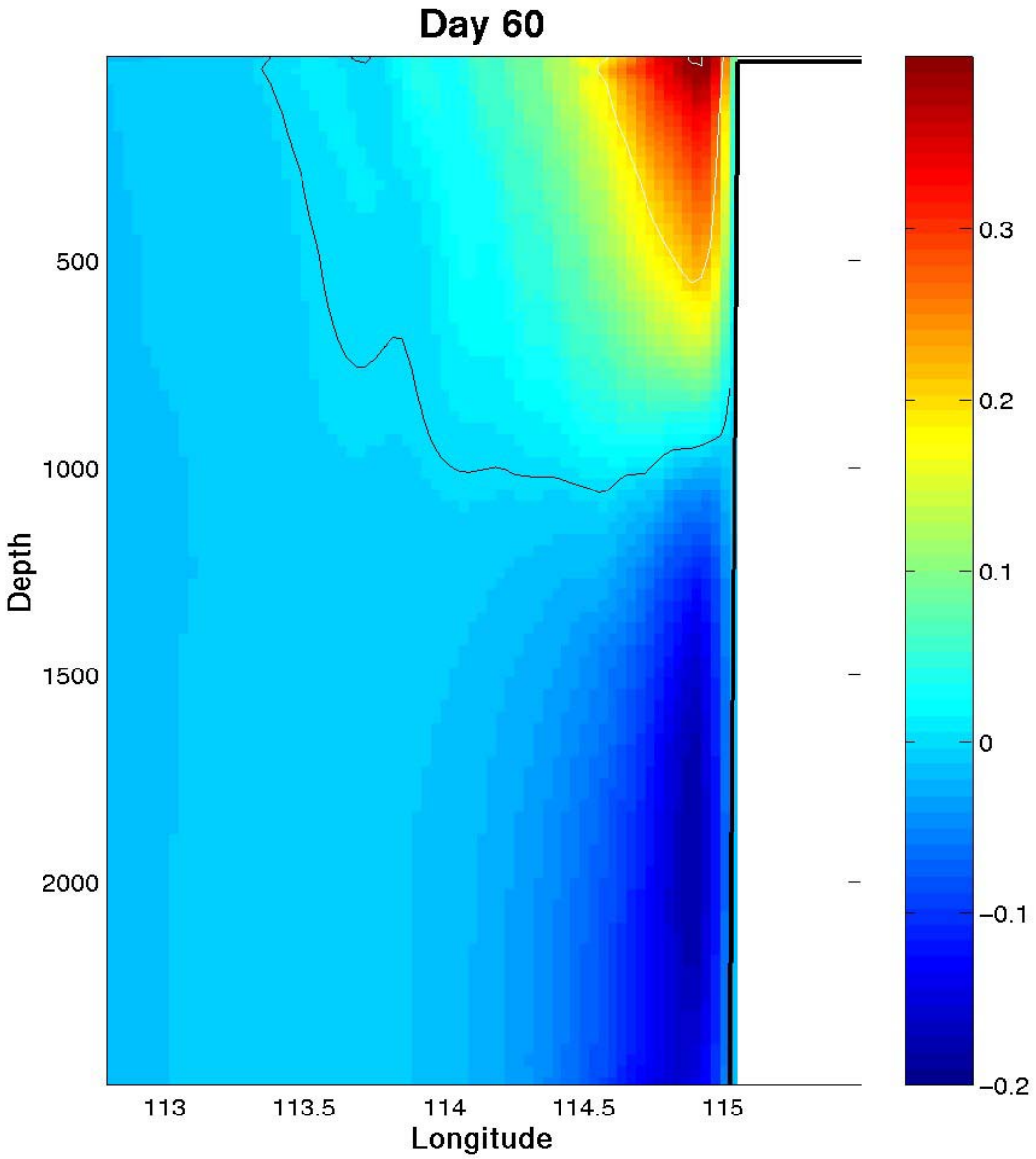

Figure 10d. Cross-section of north-south velocities (m/s) at Cape Leeuwin (34.3°S) for Experiment 2 on day 60. Blue is poleward (south).

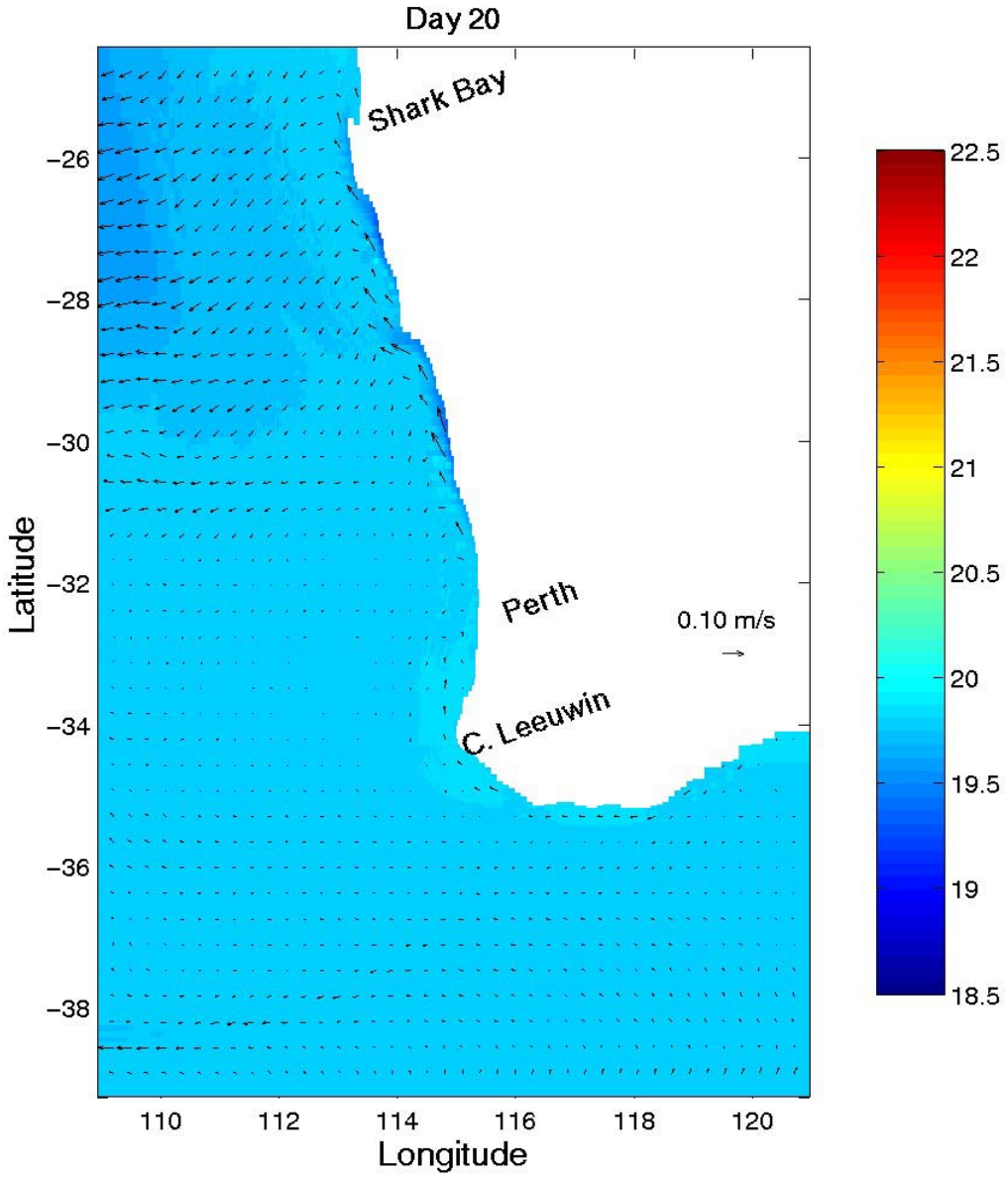

Figure 11a. Surface temperatures (°C) and velocity vectors for Experiment 3 on day 20.

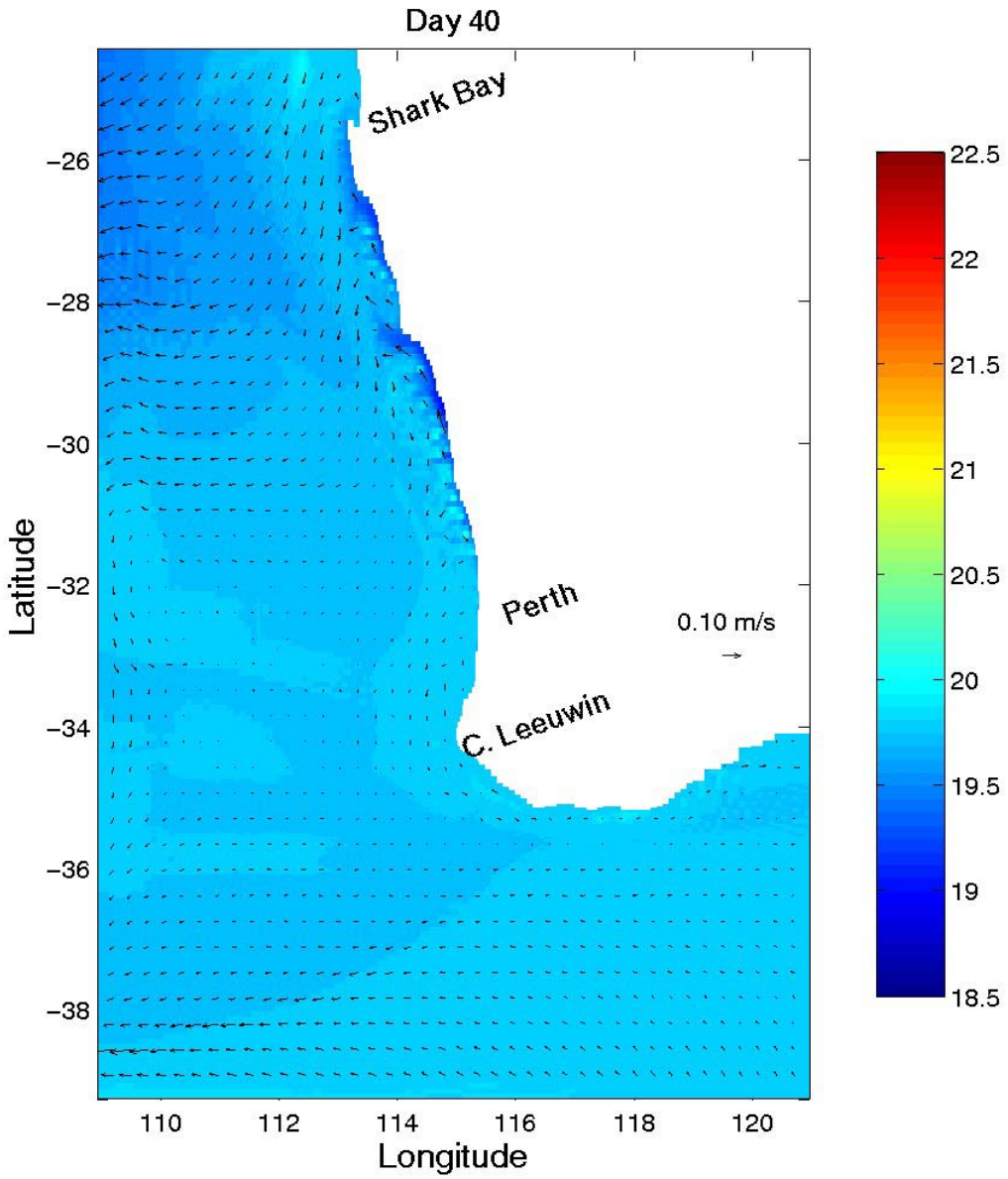

Figure 11b. Surface temperatures (°C) and velocity vectors for Experiment 3 on day 40.

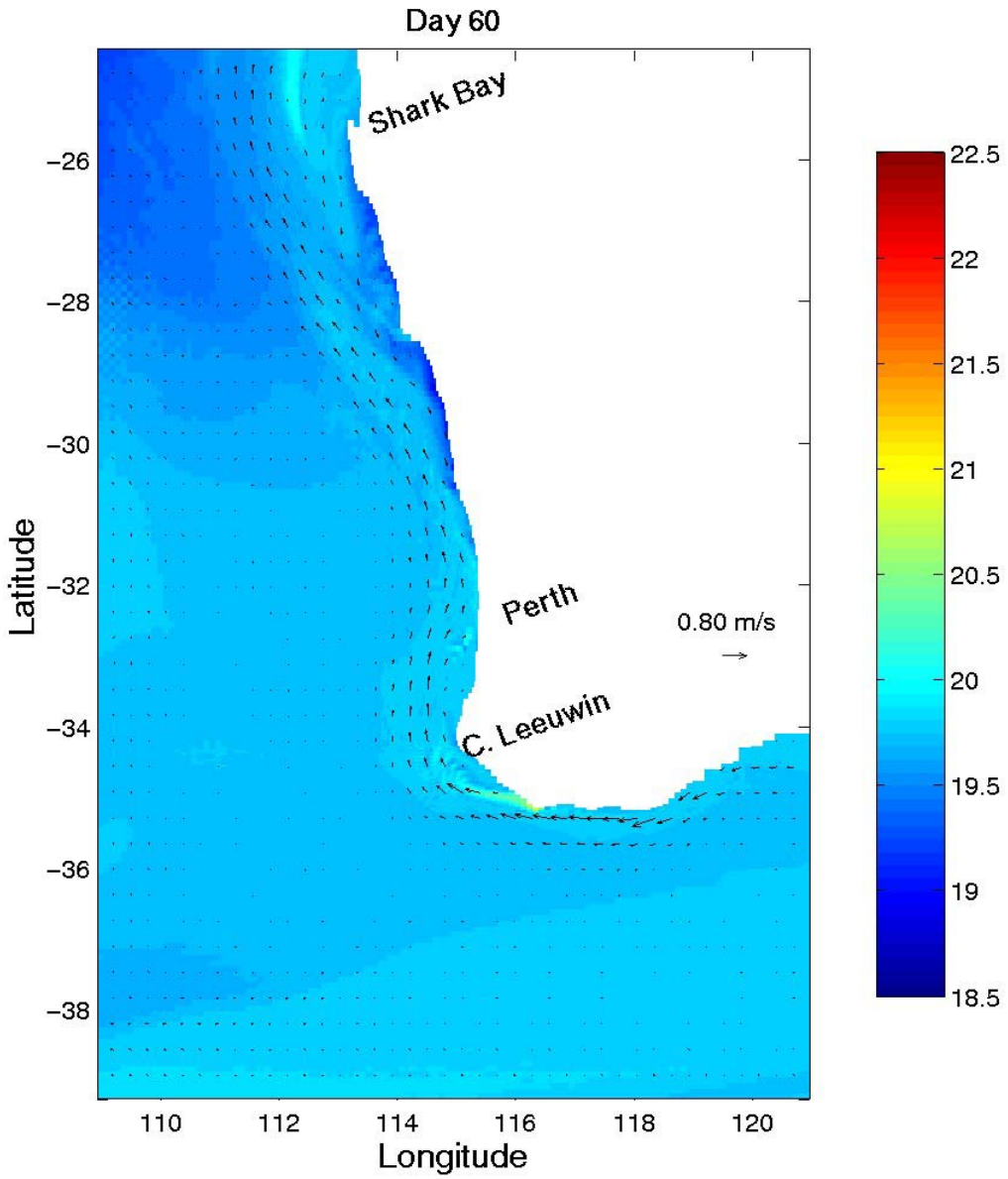

Figure 11c. Surface temperatures (°C) and velocity vectors for Experiment 3 on day 60.

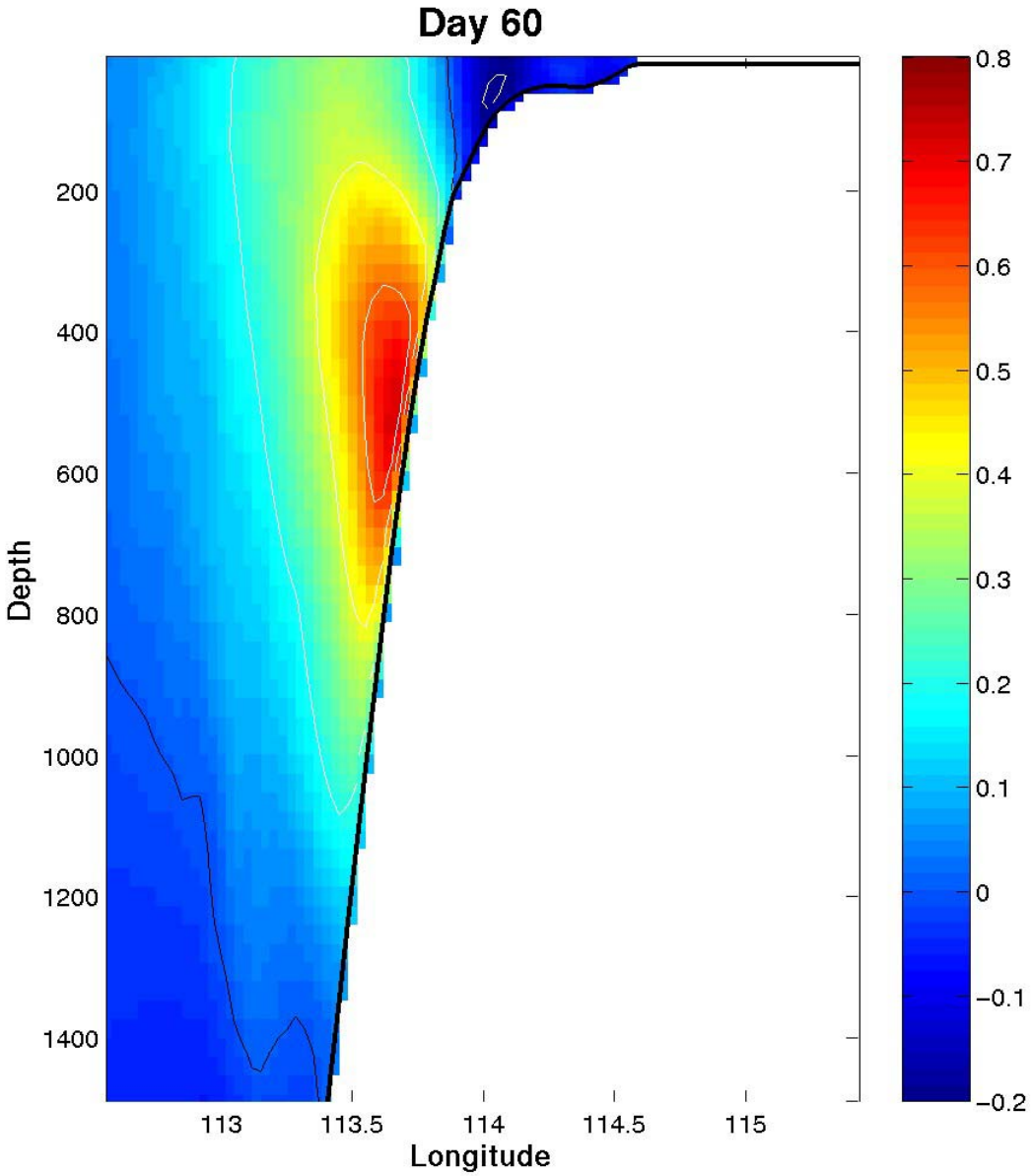

Figure 11d. Cross-section of north-south velocities (m/s) at 29°S for Experiment 3 on day 60. Blue is poleward (south).

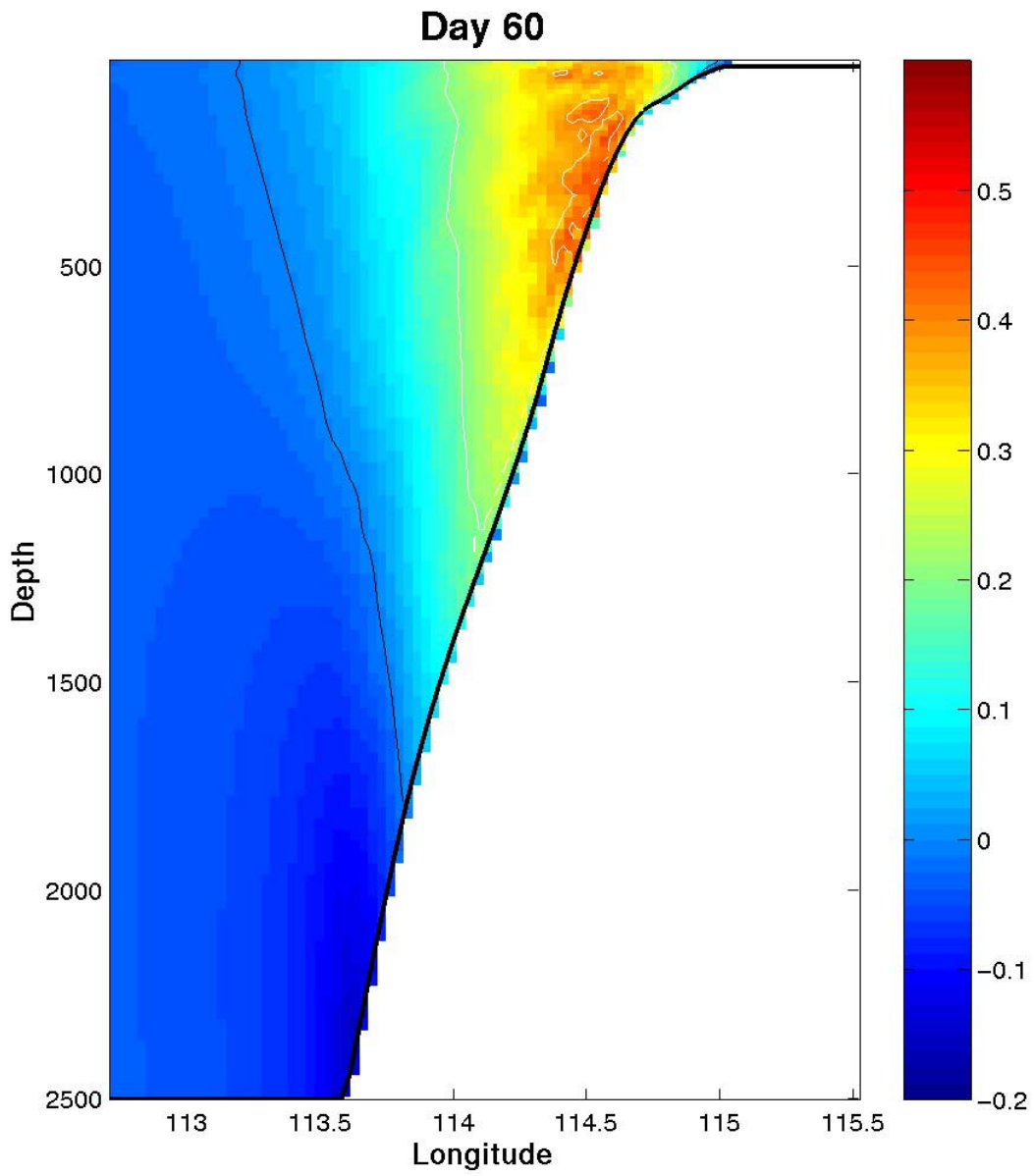

Figure 11e. Cross-section of north-south velocities (m/s) at Cape Leeuwin (34.3°S) for Experiment 3 on day 60. Blue is poleward (south).

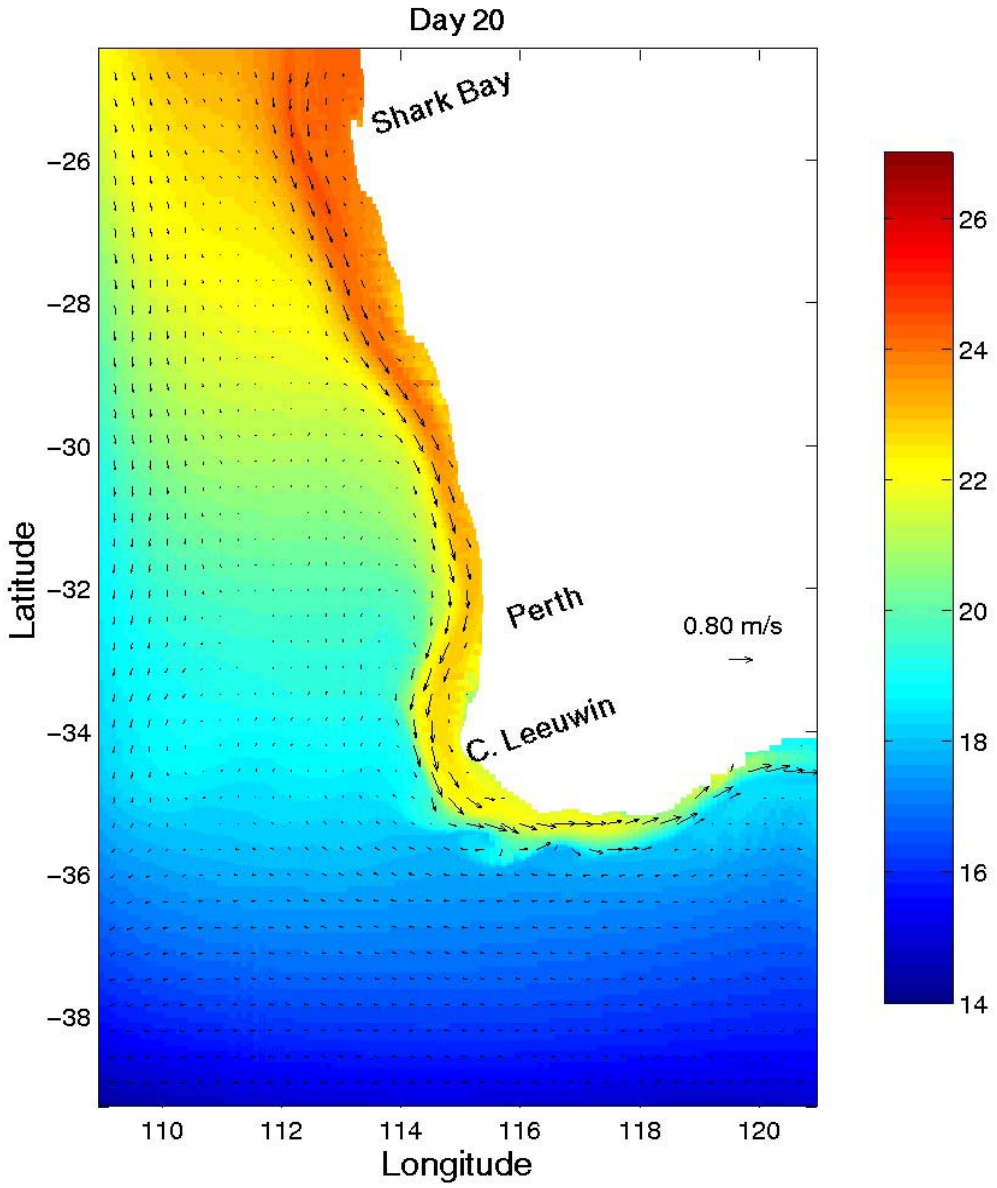

Figure 12a. Surface temperatures (°C) and velocity vectors for Experiment 4 on day 20.

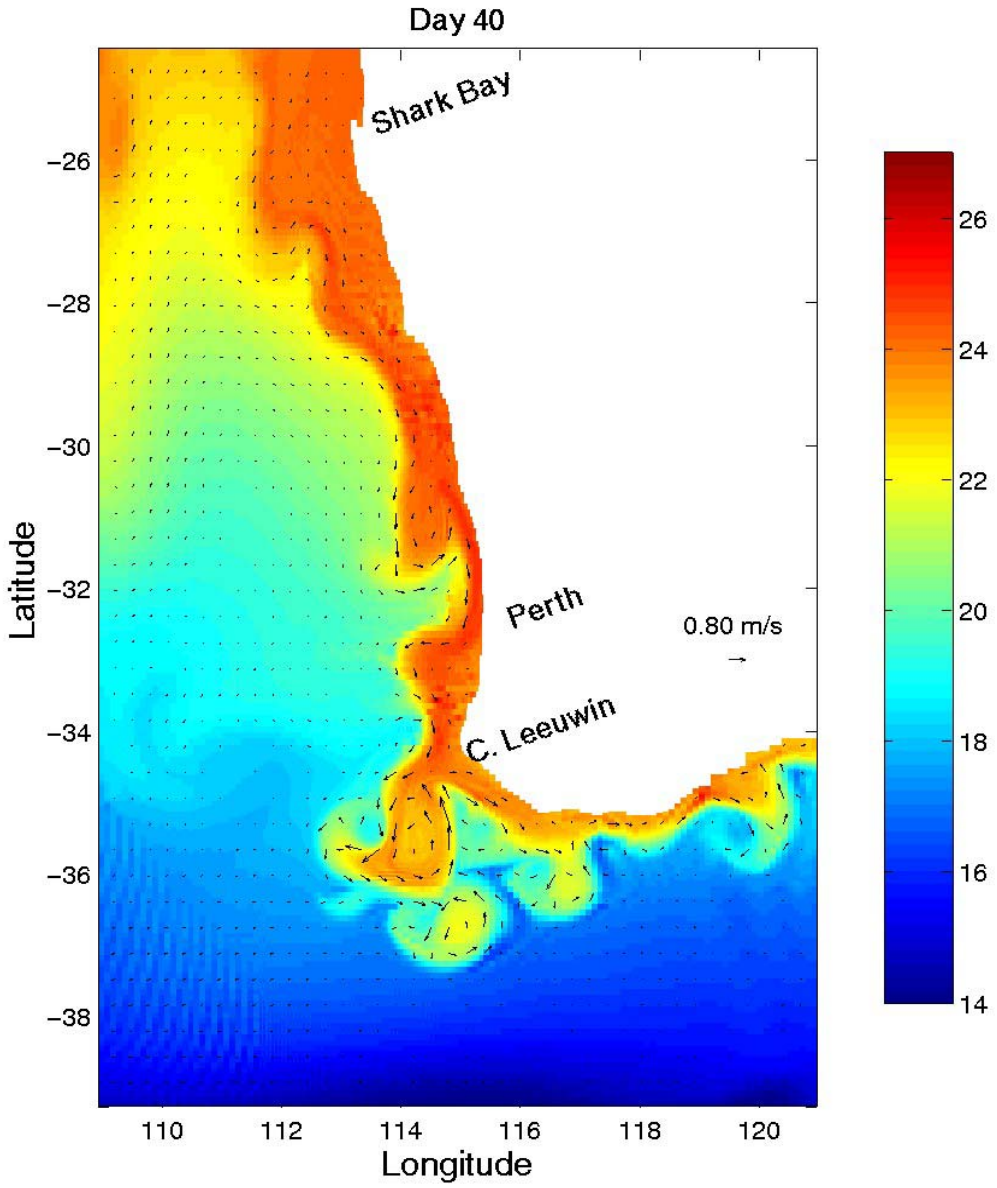

Figure 12b. Surface temperatures (°C) and velocity vectors for Experiment 4 on day 40.

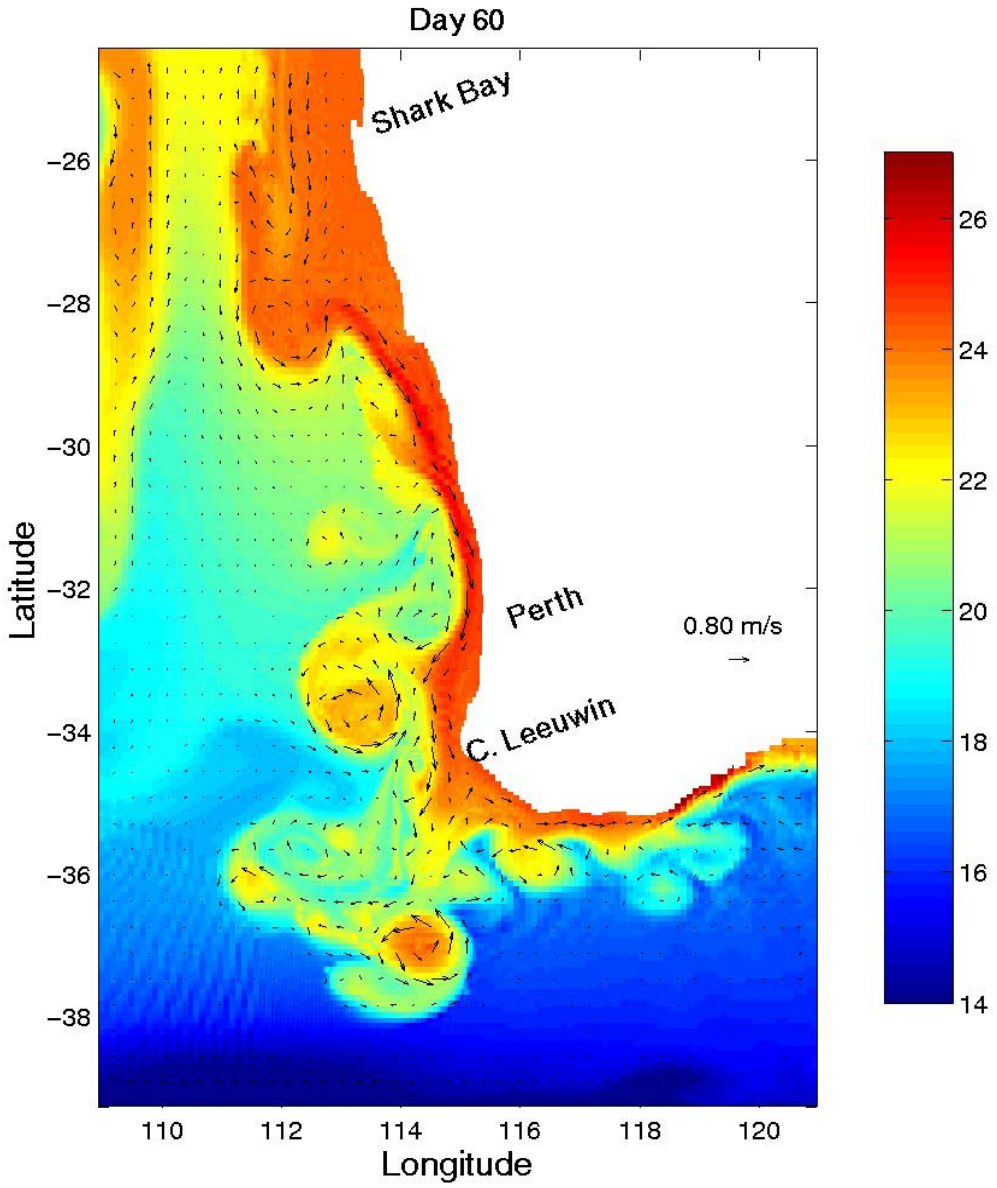

Figure 12c. Surface temperatures (°C) and velocity vectors for Experiment 4 on day 60.

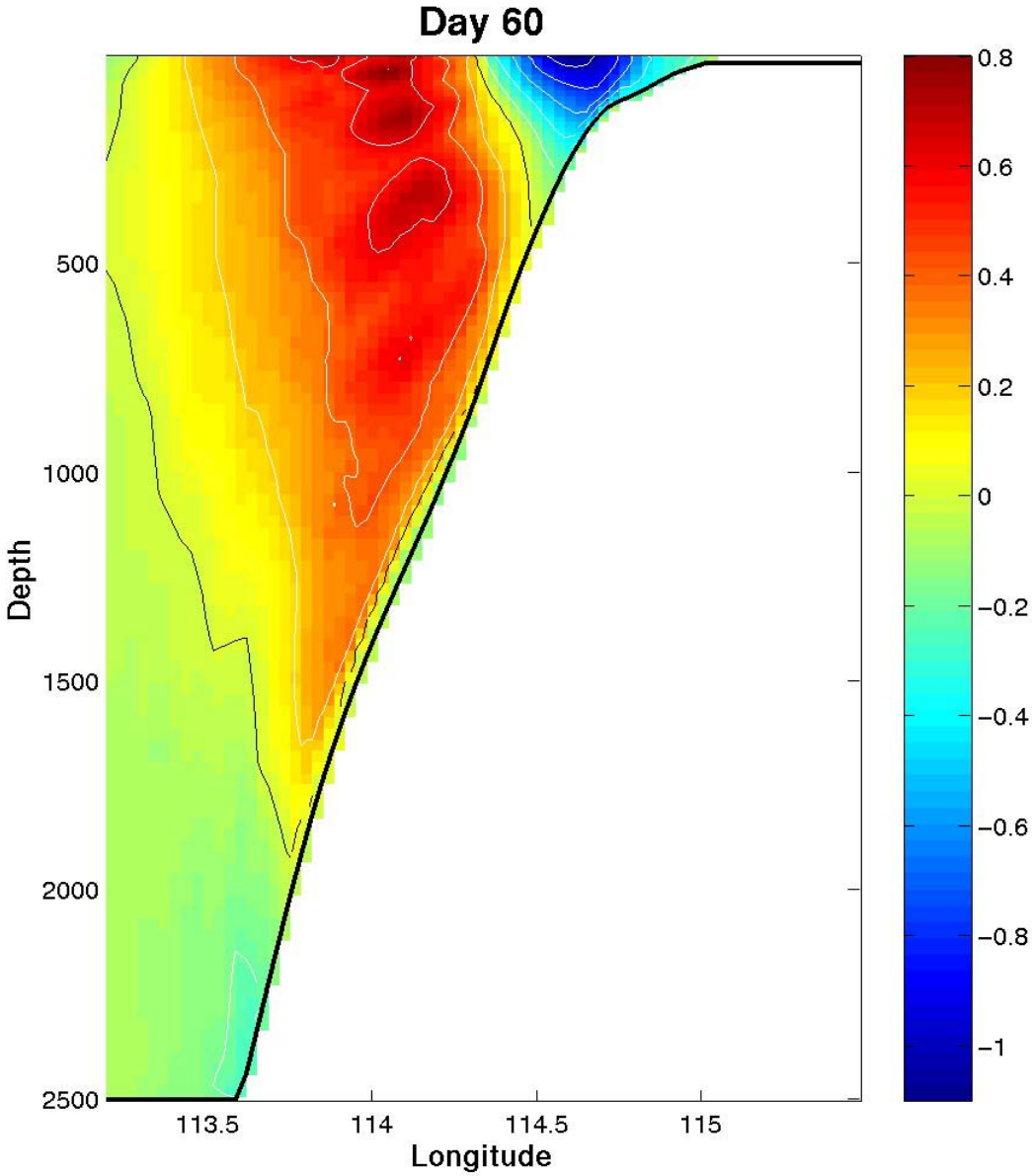

Figure 12d. Cross-section of north-south velocities (m/s) at Cape Leeuwin (34.3°S) for Experiment 4 on day 60. Blue is poleward (south).

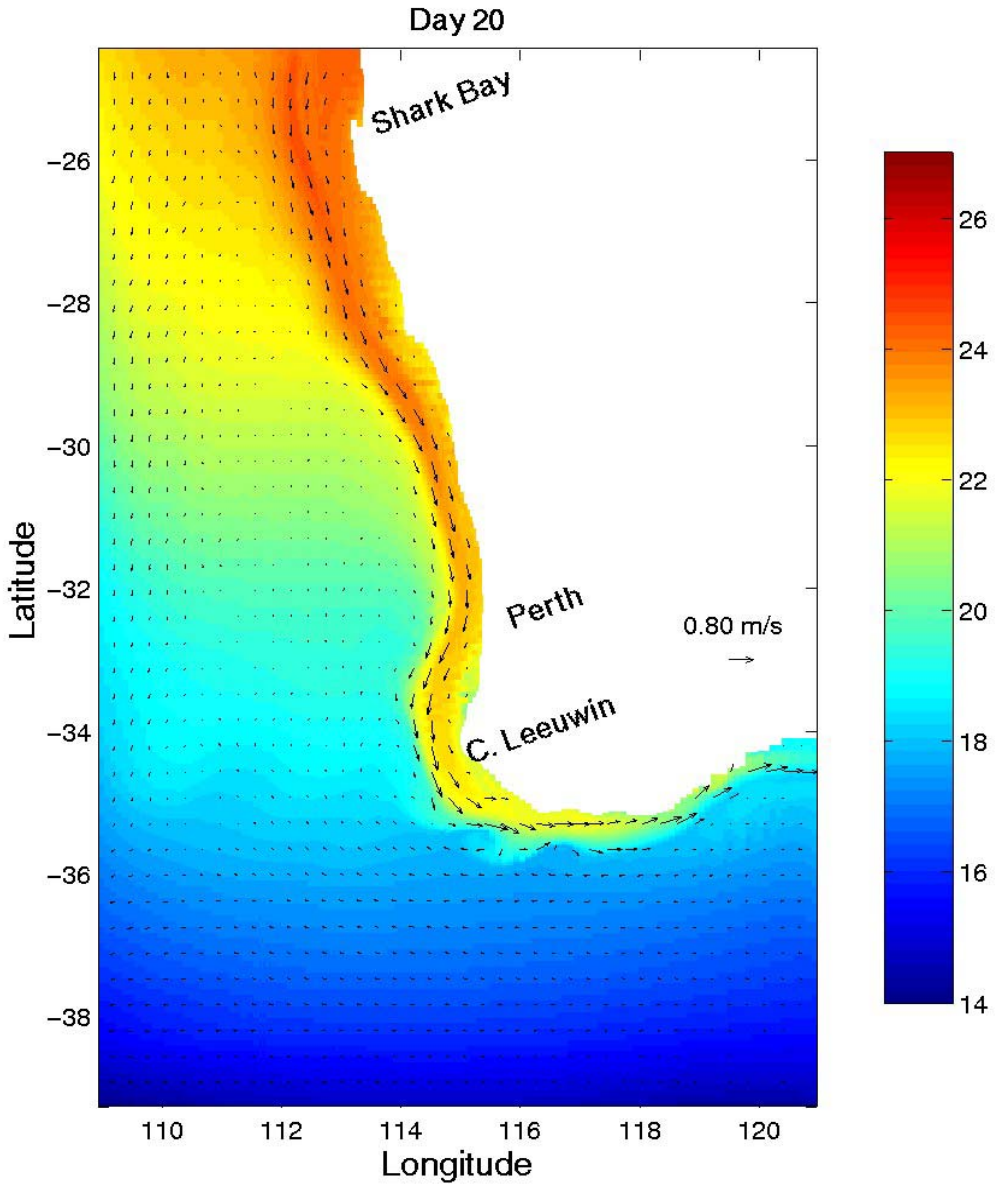

Figure 13a. Surface temperatures (°C) and velocity vectors for Experiment 5 on day 20.

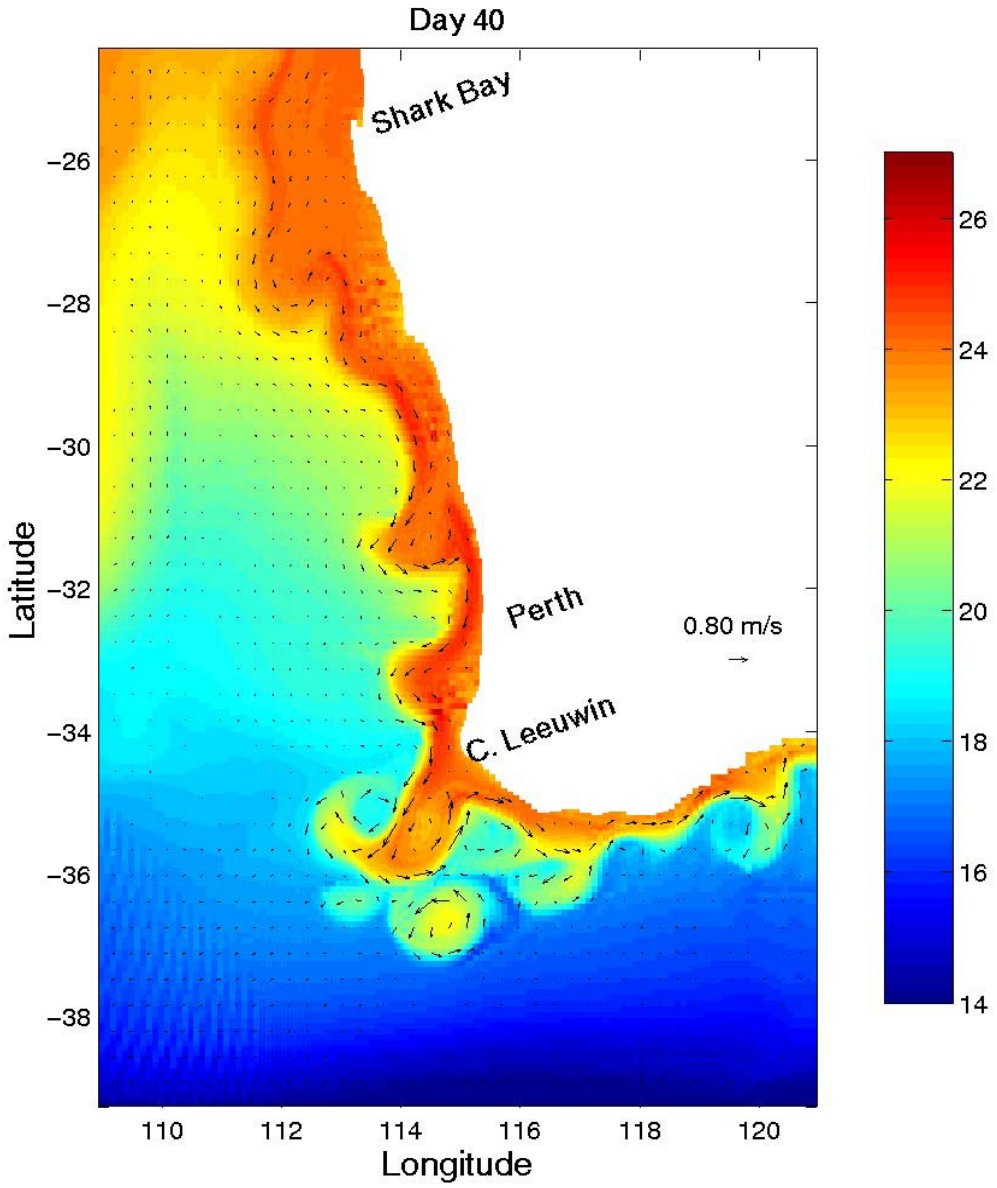

Figure 13b. Surface temperatures (°C) and velocity vectors for Experiment 5 on day 40.

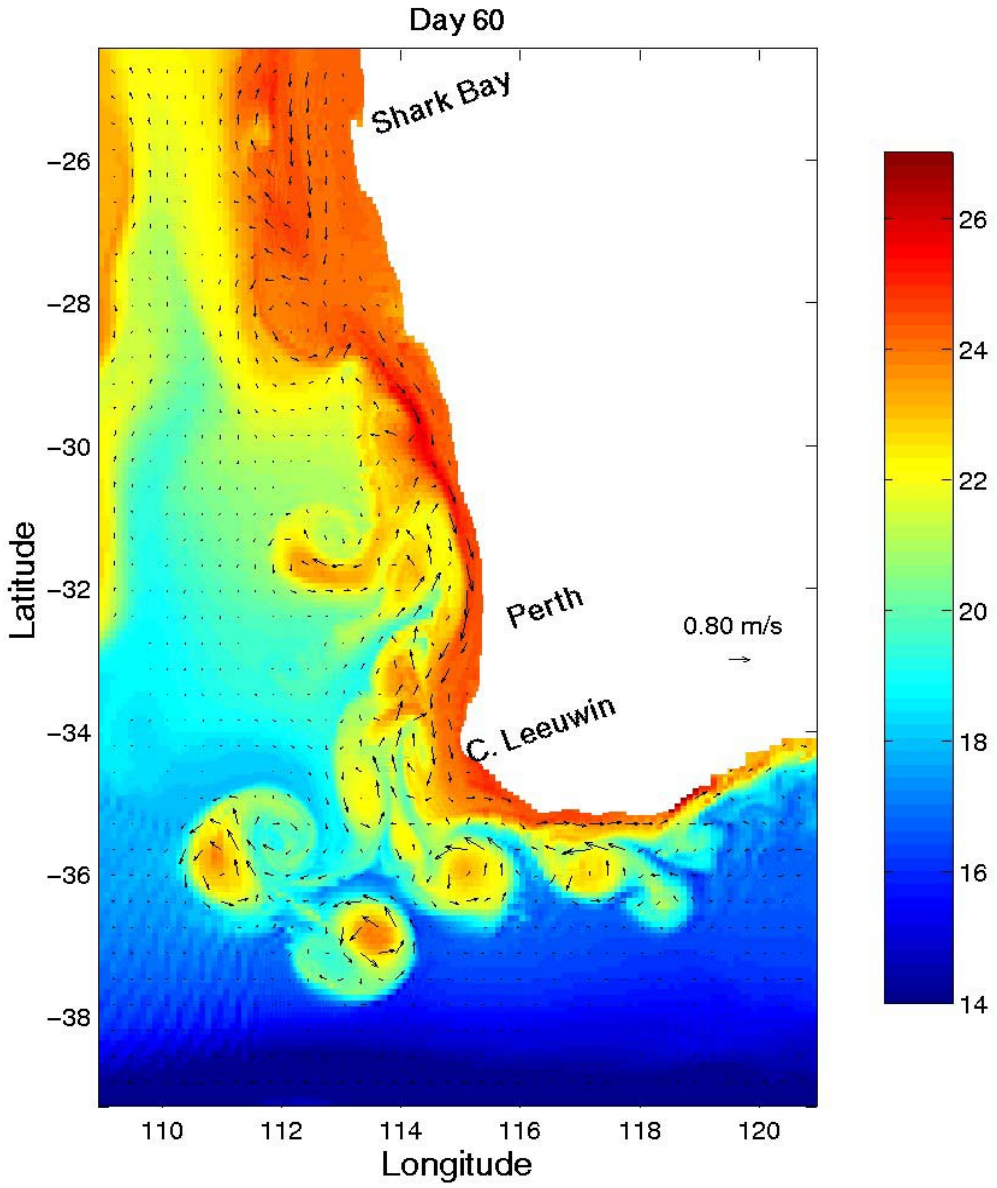

Figure 13c. Surface temperatures (°C) and velocity vectors for Experiment 5 on day 60.

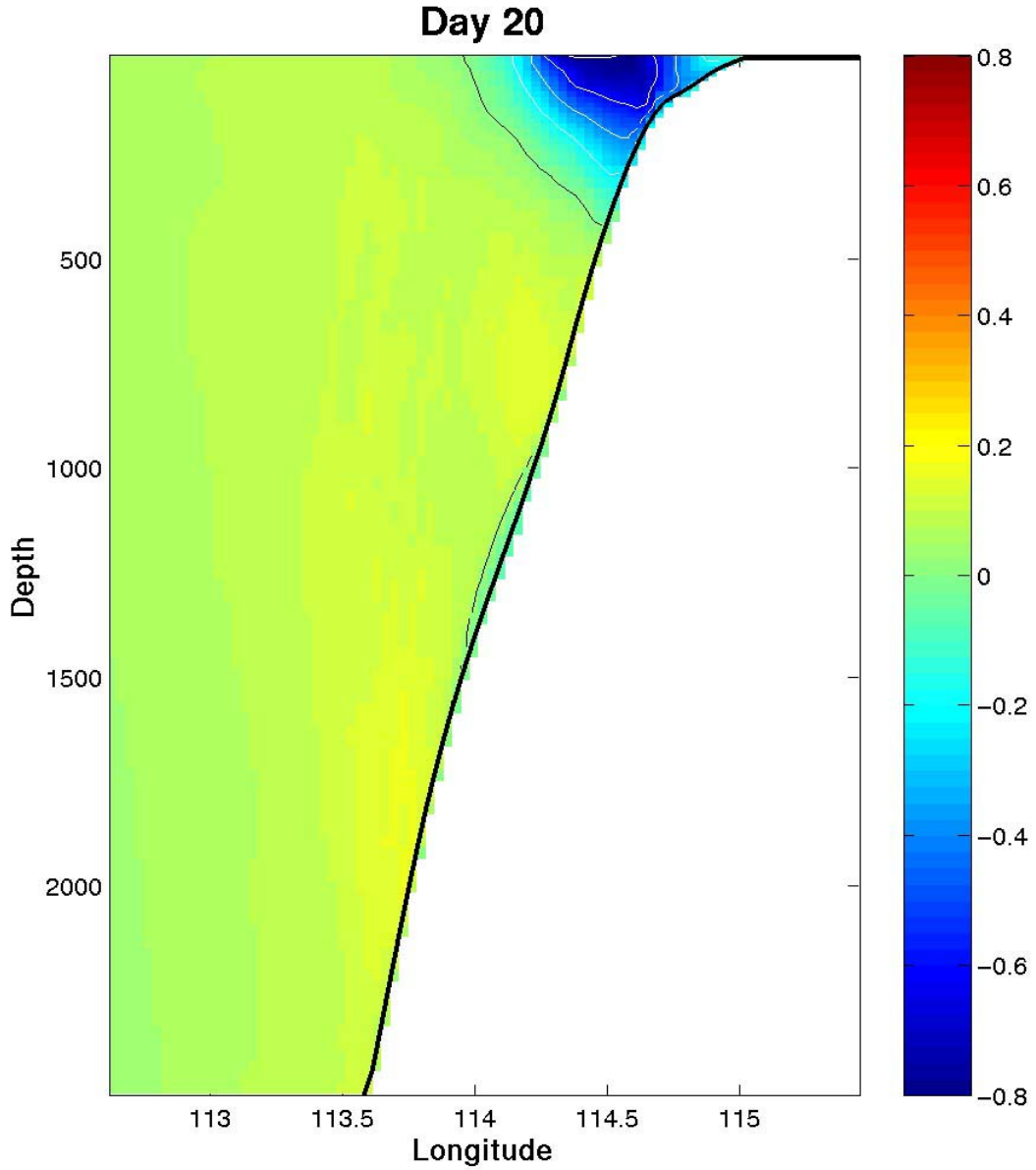

Figure 13d. Cross-section of north-south velocities (m/s) at Cape Leeuwin (34.3°S) for Experiment 5 on day 20. Blue is poleward (south).

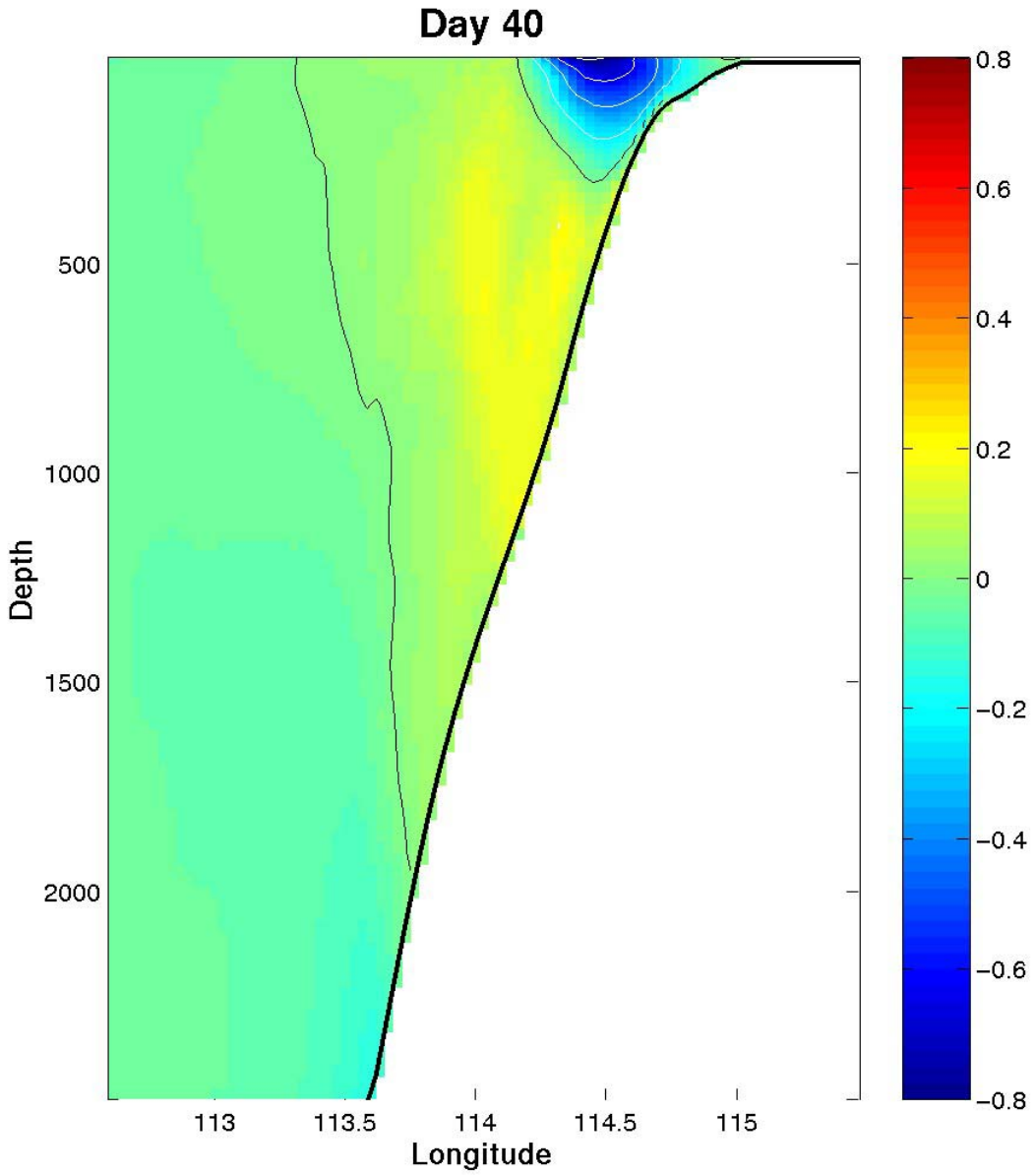

Figure 13e. Cross-section of north-south velocities (m/s) at Cape Leeuwin (34.3°S) for Experiment 5 on day 40. Blue is poleward (south).

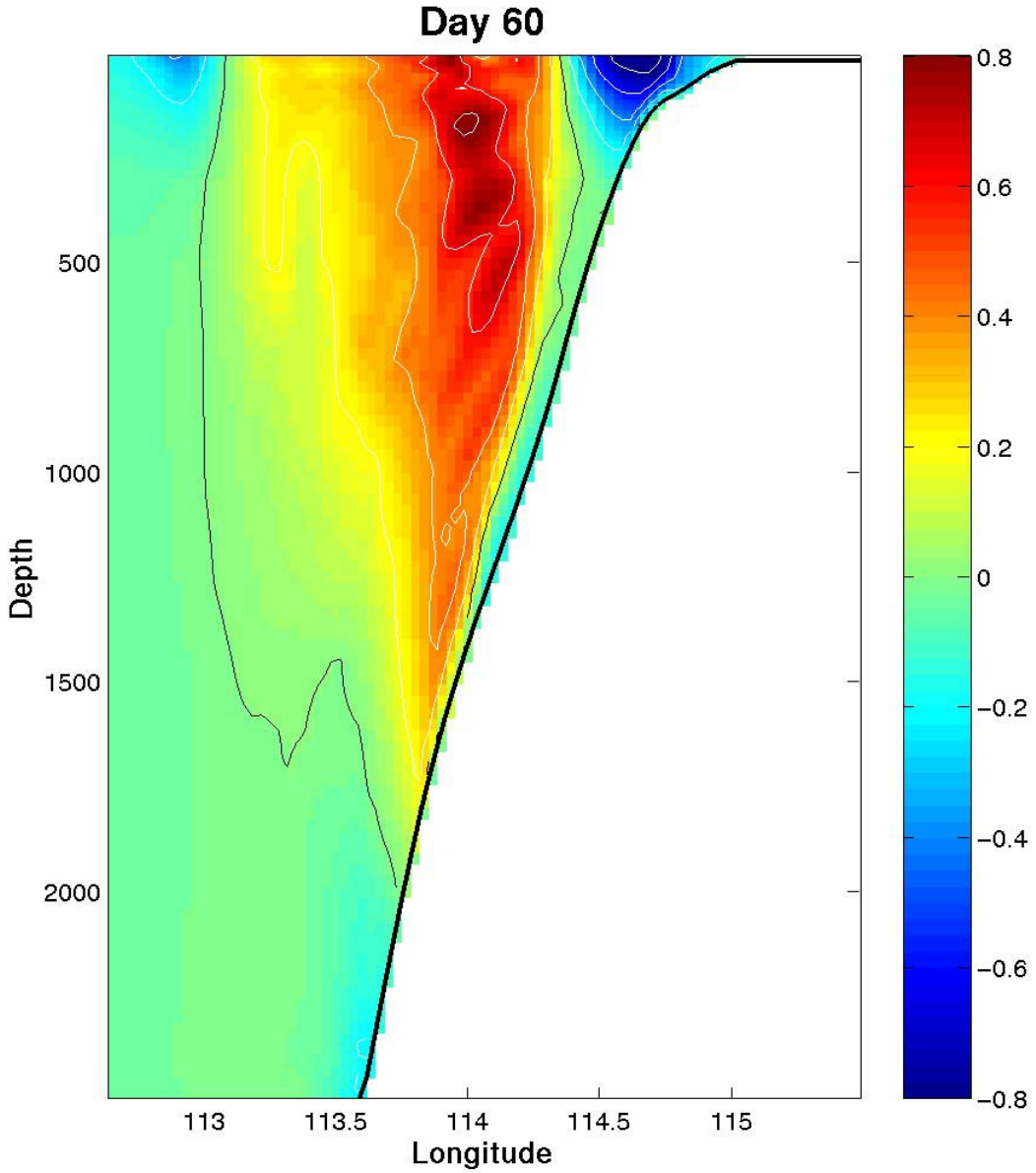

Figure 13f. Cross-section of north-south velocities (m/s) at Cape Leeuwin (34.3°S) for Experiment 5 on day 60. Blue is poleward (south).

Exp #	Annual Wind	Climatology	Topography
1	NO	HORIZONTALLY AVERAGED	YES
2	YES	HORIZONTALLY AVERAGED	NO
3	YES	HORIZONTALLY AVERAGED	YES
4	NO	FULL	YES
5	YES	FULL	YES

Table 1. Summary of experimental design

Level	Depth (m)	Level	Depth (m)	Level	Depth (m)
1	0	12	300	23	1400
2	10	13	400	24	1500
3	20	14	500	25	1750
4	30	15	600	26	2000
5	50	16	700	27	2500
6	75	17	800	28	3000
7	100	18	900	29	3500
8	125	19	1000	30	4000
9	150	20	1100	31	4500
10	200	21	1200	32	5000
11	250	22	1300	33	5500

Table 2. Vertical levels and depths used by Levitus and Boyer (1994) and Levitus et al. (1994)

Level	Sigma Value	Level	Sigma Value
1	0	12	-0.61538
2	-0.00961	13	-0.69231
3	-0.01923	14	-0.76923
4	-0.03846	15	-0.84615
5	-0.07692	16	-0.92308
6	-0.15385	17	-0.96154
7	-0.23077	18	-0.98077
8	-0.30769	19	-0.99038
9	-0.38462	20	-0.99519
10	-0.46154	21	-1.0
11	-0.53846		

Table 3. Values of sigma levels

LIST OF REFERENCES

Batteen, M. L. and C. L. Butler, Modeling Studies of the Leeuwin Current Off Western and Southern Australia, *J. Phys. Oceanography*, 28, 2199-2221, 1998.

Batteen, M. L., M. J. Rutherford, and E. J. Bayler, A Numerical Study of Wind and Thermal Forcing Effects on the Ocean Circulation Off Western Australia, *J. Phys. Oceanography*, 22, 1406-1433, 1992.

Blumberg, A. F., and G. L. Mellor, A Description of a Three-Dimensional Coastal Ocean Circulation Model, In: *Three-Dimensional Coastal Ocean Models, Coastal Estuarine Sci*., 4, edited by N. Heaps, pp 1-16, AGU, Washington, DC, 1987.

Chapman, D. C., Numerical Treatment of Cross-Shelf Open Boundaries in a Barotropic Coastal Ocean Model, *Journal of Phys. Oceanography*, 25, 1060-1075, 1985.

Church, J. A., G. R. Cresswell, and J. S. Godfrey, The Leeuwin Current. In: *Poleward Flows Along Eastern Ocean Boundaries*, S. Neshhyba, C. N. K. Moorers, R. I. Smith, and R. T. Barber, Eds., Springer-Verlag, 230-252, 1989.

Cresswell, G. R. and T. J. Golding, Observations of a South-Flowing Current in the Southeastern Indian Ocean, *Deep-Sea Res.*, 27A, 449-466, 1980.

Cresswell, G. R. and J. L. Peterson, The Leeuwin Current South of Western Australia, *Aust. J. Mar. Freshwater Res.*, 44, 285-303, 1993.

Ezer, T. and G. L. Mellor, Diagnostic and Prognostic Calculations of the North Atlantic Circulation and Sea Level Using a Sigma Coordinate Ocean Model, *J. of Geophys. Res.*, 99(C7), 14159-14171, 1994.

Ezer, T. and G. L. Mellor, Simulations of the Atlantic Ocean With a Free Surface Sigma Coordinate Ocean Model, *J. of Geophys. Res.*, 102(C7), 15647-15657, 1997.

Godfrey, J. S. and K. R. Ridgway, The Large-Scale Environment of the Poleward-Flowing Leeuwin Current, Western Australia: Longshore Steric Height Gradients, Wind Stresses and Geostrophic Flow, *J. Phys. Oceanography*, 15, 481-495, 1985.

Godfrey, J. S., D. J. Vaudrey, and S. D. Hahn, Observations of the Shelf-Edge Current South of Australia Winter 1982, *J. Phys. Oceanography*, 16, 668-679, 1986.

Hirst, A. C., and J. S. Godfrey, The role of Indonesian Throughflow in a Global Ocean GCM, *J. Phys. Oceanography*, 23,1057-1086, 1993.

Levitus, S., and T. P. Boyer, World Ocean Atlas 1994, Vol. 4: Temperature, *NOAA Atlas NESDI 4*, 117 pp., U. S. Dept. of Commerce, Washington, D.C., 1994.

Levitus, S., R. Burgett, and T. P. Boyer, World Ocean Atlas 1994, Vol. 3: Salinity, *NOAA Atlas NESDI 3*, 99 pp., U. S. Dept. of Commerce, Washington, D.C., 1994.

Marchesiello, P., J. C. McWilliams, and A. Shchepetkin, Open Boundary Conditions for Long-Term Integration of Regional Oceanic Models, *Ocean Modeling*, 3, 1-20, 2001.

Martinho, A. C., A Fine Resolution Model of the Coastal Eastern Boundary Current Systems Off Iberia and Morocco, Masters Thesis, Naval Postgraduate School, Monterey, CA, 93 pp, 2001.

McCreary, J. P., S. R. Shetye, and P. K. Kundu, Thermohaline Forcing of Eastern Boundary Currents: With Application to the Circulation Off the West Coast of Australia, *J. Mar. Res.*, 44, 71-92, 1986.

Mellor, G. L., User’s guide for a Three-Dimensional, Primitive Equation, Numerical Ocean Model, 40 pp, Program in Atmos. And Ocean Sci. Report, Princeton Univ., Princeton, NJ 1996.

Mellor, G. L., L. Y. Oey, and T. Ezer, Sigma Coordinate Pressure Gradient Errors and the Seamount Problem, *J. Atmospheric and Ocean Technology*, 15, 1122-1131, 1998.

Mellor, G. L., and T. Yamada, Development of a Turbulence Closure Model for Geophysical Fluid Problems, *Rev. Geophys. Space Phys*., 20, 851-875, 1982.

Palma, E. D., and R. P. Matano, On the Implementation of Passive Open Boundary Conditions for a General Circulation Model: the Barotropic Mode, *J. Geophys. Res.*, 103(C1), 1319-1341, 1998.

Palma, E. D., and R. P. Matano, On the Implementation of Passive Open Boundary Conditions for a General Circulation Model: the Three-Dimensional Case, *Journal of Geophysical Research*, 105(C4), 8605-8627, 2000.

Parrish, R. H., A. Bakun, D. M. Husby, and C. S. Nelson, Comparitive Climatology of Selected Environmental Processes in Relation to Eastern Boundary Current Pelagic Fish Reproduction. In: *Proc. Expert Consultation to Examine Changes in Abundance and Species of Neritic Fish Resources*, G. D. Sharp and J. Csirke, Eds., San Jose, Costa Rica, FAO Fish Rep. 291, Vol. 3, 731-778, 1983.

Sandwell, D. T., and W. F. Smith, Global Bathymetric Prediction for Ocean Modeling and Marine Geophysics, 1996.

Smagorinsky, J., S. Manabe, and J. L. Holloway, Numerical Results From a Nine-Level General Circulation Model of the Atmosphere, *Mon. Weather Rev.,* 93, 727-768, 1965.

Smith, R. L., A. Huyer, J. S. Godfrey, and J. A. Church, The Leeuwin Current Off Western Australia, 1986-1987, *J. Phys. Oceanography*, 21, 323-345, 1991.

Thompson, R. O. R. Y., Observations of the Leeuwin Current Off Western Australia, *J. Phys. Oceanography*, 14, 623-628, 1984.

Thompson, R. O. R. Y., Continental-Shelf Scale Model of the Leeuwin Current, *J. Mar. Res.*, 45, 813-827, 1987.

Trenberth, K. E., W. G. Large, J. G. Olsen, The Mean Annual Cycle in Global Ocean Wind Stress, *J. Phys. Oceanography*, 20, 1742-1760, 1990.

Tworek, T. J., The Role of the Planetary Beta Effect on Currents and Eddies in the Leeuwin Current System, Masters

Thesis, Naval Postgraduate School, Monterey, CA, 163 pp, 2000.

INITIAL DISTRIBUTION LIST

1. Defense Technical Information Center
   Ft. Belvoir, VA

2. Dudley Knox Library
   Naval Postgraduate School
   Monterey, CA

3. Chairman, Department of Oceanography
   (Code OC/Bv)
   Naval Postgraduate School
   Monterey, CA

4. Chairman, Department of Meteorology
   (Code MR/Wx)
   Naval Postgraduate School
   Monterey, CA

5. Dr. Mary L. Batteen (Code OC/Bv)
   Naval Postgraduate School
   Monterey, CA

6. Dr. Robert Bourke (Code OC/Bf)
   Naval Postgraduate School
   Monterey, CA

7. LT Scott Boedeker
   9446 Hito Ct
   San Diego, CA 92129

8. Antonio Martinho
   5200 Coe Ave. Apt. # 1155
   Seaside, CA 93955